Bulletin of Volcanology (2018) 80:80
https://doi.org/10.1007/s00445-018-1254-9

RESEARCH ARTICLE

# Widespread tephra layers in the Bering Sea sediments: distal clues to large explosive eruptions from the Aleutian volcanic arc

A. N. Derkachev[1] · V. V. Ponomareva[2] · M. V. Portnyagin[3,4] · S. A. Gorbarenko[1] · N. A. Nikolaeva[1] · M. I. Malakhov[5] · E. A. Zelenin[6] · D. Nürnberg[3] · Yanguang Liu[7]

Received: 26 March 2018 / Accepted: 9 October 2018


## Abstract

Tephra layers within marine sediments provide information on past explosive eruptions, which is especially important in the case of remote island arcs where data on proximal pyroclastic deposits can be scarce. Three Alaska-Aleutian tephras (labeled Br2, SR2, and SR4) were found in the late Pleistocene-Holocene sediments of the Bering Sea (north Pacific). We fingerprint glass from these tephras with the help of single-shard electron microprobe and LA-ICP-MS analyses and provide microprobe data on minerals from two of these tephras. The large compositional variability of the Alaska-Aleutian volcanoes permits the use of ratios of highly incompatible trace elements (Ba/Nb, Th/Nb, Th/La, La/Nb) for identification of distal tephra sources by comparison of these ratios in tephra glass and proximal bulk rock analyses. This method, along with mapped tephra dispersal, has allowed us to link tephras under study to Aniakchak, Semisopochnoi, and Okmok volcanoes, respectively. Our results indicate that tephra Br2 was derived from the ~3.6 ka Aniakchak II caldera-forming eruption (Alaska, USA). This is the first ever finding of the Aniakchak II tephra in Bering Sea sediments, which permits enlargement of its tephra volume and eruption magnitude to ~100 km$^3$ and 6.8, respectively. Tephra SR2, dated at ~12.2 ka, is likely associated with a post-glacial caldera on the Semisopochnoi Island, Aleutians (USA). Tephra SR4 (dated at ~64.5 ka), likely was derived from an earlier undocumented eruption from Okmok volcano (Aleutians). All three regionally spread tephra layers are valuable isochrones, which can be used for correlating and dating of Bering Sea sediments.

**Keywords** North Pacific · Late Quaternary · Marine tephrochronology · Volcanic glass chemistry · Electron microprobe · LA-ICP-MS

M. I. Malakhov died before publication of this work was completed.

Editorial responsibility: R.J. Brown

**Electronic supplementary material** The online version of this article (https://doi.org/10.1007/s00445-018-1254-9) contains supplementary material, which is available to authorized users.

✉ V. V. Ponomareva
ponomareva@kscnet.ru; vera.ponomareva1@gmail.com

[1] V.I. Il'ichev Pacific Oceanological Institute, 43 Baltiyskaya St, Vladivostok 690041, Russia

[2] Institute of Volcanology and Seismology, Piip Blvd. 9, Petropavlovsk-Kamchatsky 683006, Russia

[3] GEOMAR Helmholtz Centre for Ocean Research Kiel, Wischhofstrasse, 1-3, 24148 Kiel, Germany

[4] V.I. Vernadsky Institute of Geochemistry and Analytical Chemistry, Kosygin St. 19, Moscow 119991, Russia

[5] North-East Interdisciplinary Science Research Institute, Portovaya St. 16, Magadan 685000, Russia

[6] Geological Institute, Pyzhevsky Lane 7, Moscow 119017, Russia

[7] First Institute of Oceanography, SOA, Xian-Xia-Ling Road, 6, Qingdao 266061, China

Published online: 30 October 2018

## Introduction

Tephra layers found in marine and terrestrial sediments inform about past explosive eruptions and serve as excellent marker horizons for correlating disparate sedimentary archives and dating past geological events (e.g., Shane 2000; Lowe 2011; Davies et al. 2016; Blockley et al. 2014; Ponomareva et al. 2015a, 2015b). Non-erosive marine environments provide better tephra archives than terrestrial environments where pyroclastic deposits often form complex successions and can be partly or completely eroded especially in glaciated or coastal areas (Rawson et al. 2015). Therefore, marine tephras are a key tool in the reconstruction of past explosive eruptions and for establishing their age and magnitude (e.g., Alloway et al. 2005; Kutterolf et al. 2008a, 2008b; Shane and Wright 2011; Costa et al. 2014). This is particularly true for the island arcs where a substantial portion of the erupted pyroclastic material can be dispersed over water.

The Aleutian volcanic arc (Fig. 1) has a long history of explosive volcanism, which is testified by the presence of many calderas (Miller and Smith 1987; Cameron and Nye 2014) and by numerous tephra layers in the Alaskan terrestrial sediments downwind from the arc (e.g., Preece et al. 1999, 2011a, 2011b; Westgate et al. 2000; Jensen et al. 2008, 2011, 2013; Davies et al. 2016). Most of these tephra layers have not been linked to their parent eruptions, as those remain undocumented in proximal records (Preece et al. 2011b). The volumes of known large eruptions have been crudely estimated based on caldera size, thickness, and distribution of associated ignimbrites, and by comparison to better studied calderas in other volcanic zones (Miller and Smith 1987). However, most of these estimates do not include distal tephra, which may constitute a significant part of the erupted products, and so the tephra volumes and magnitudes of many eruptions may have been underestimated.

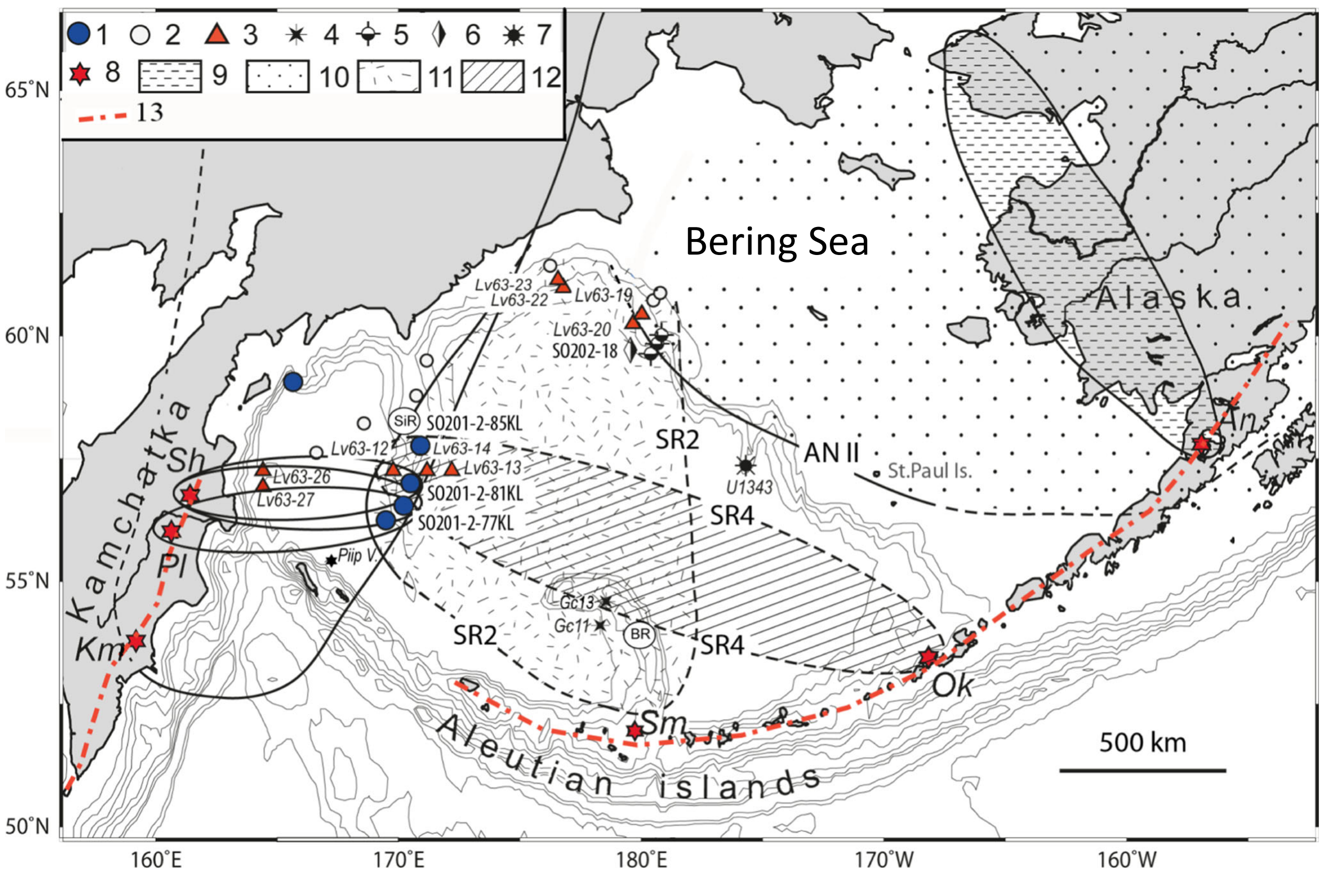


**Fig. 1** Map showing locations of the Bering Sea sediment cores considered in this paper and dispersal areas of major ash falls in the area. 1–7 Locations of coring sites; 1–2 research vessel (R/V) "Sonne" Leg SO201-2 cores (Dullo et al. 2009): 1—with tephra layers, 2—without tephra layers; 3—R/V "Akademik Lavrentyev" (Lv63); 4—R/V "Akademik A. Vinogradov" (Gc, Gorbarenko et al. 2010); 5—R/V "MIRAI" (Harada 2006); 6—R/V "Sonne," INOPEX, Gersonde 2012); 7—IODP Expedition 323 (Expedition 323…2010; Takahashi et al. 2011); 8—known source volcanoes for Bering Sea tephra: *Sh* Shiveluch, *Pl* Plosky volcanic massif, *Km* Karymsky eruptive center, *Sm* Semisopochnoi, *Ok* Okmok, *An* Aniakchak. 9–12—dispersal areas of tephra; 9–10—tephra from the ~3.6 ka Aniakchak II caldera-forming eruption (Alaska); 9—earlier mapped by Davies et al. 2016; 10—this study, Graham et al. 2016, Ponomareva et al. 2018; 11—SR2 tephra from Semisopochnoi volcano; 12—SR4 tephra from Okmok volcano. Other lines and ovals show dispersal of the Rauchua (SR6) tephra, and tephra from Plosky and Shiveluch volcanoes (Ponomareva et al. 2013a, 2013b, 2015b). 13—volcanic arcs. *BR* Bowers Ridge, *SiR* Shirshov Ridge

The Bering Sea is a key area for the reconstructions of past Alaska-Aleutian eruptions as its sediments contain numerous, but mostly unstudied, tephra layers (Creager and Scholl 1973; Seliverstov et al. 1989; Harada 2006; Dullo et al. 2009; Expedition 323 Scientists 2010; Takahashi et al. 2011; Gersonde 2012). In addition, these tephra layers could provide robust links between the disparate paleoclimate records within the Bering Sea and beyond. Only a few Bering Sea tephras have been examined to date, and all are from Kamchatka eruptions, i.e., the ~10.2 ka PL2 (SR1) tephra from the Plosky volcanic massif (Ponomareva et al. 2013a), the ~177 ka Rauchua tephra, likely from the Karymsky eruptive center (Ponomareva et al. 2013b), and several early Holocene Shiveluch tephras, admixed to PL2 layer in cores SO201-2-77 KL and -81 KL (Fig. 1; Ponomareva et al. 2015a). Unfortunately, these tephra horizons can be used for correlations only in the western part of the Bering Sea—the rest lacks geochemically fingerprinted tephra markers. Derkachev et al. (2015) described 18 < 370 ka tephra layers and lenses from 15 cores, and Aoki et al. (2012) described 48 tephras in the sedimentary core U1343 of the International Ocean Discovery Program (IODP) Leg 323, spanning the last ~2 Ma (Fig. 1; Expedition 323 Scientists 2010). However, these findings were published only as conference abstracts, thereby not allowing a complete assessment of the derived data.

In this paper, we report three widespread late Pleistocene-Holocene tephra horizons from Bering Sea sediments. Each horizon resulted from a large explosive eruption from Aleutian arc volcanoes and could serve as valuable basin-wide isochrone for paleoceanological research. These tephra layers occur in sediment cores recovered during two cruises of the research vessels (R/V) Sonne (Leg SO201-2, 2009) and Akademik Lavrentyev (Leg Lv63, 2013) (Fig. 1). Additionally, we use data on redeposited coarse tephra from cores at the foot of the Bowers Ridge (Gorbarenko et al. 2010), as well as data on pumice lapilli dredged from the submarine Piip volcano in the westernmost Aleutian arc (Yogodzinski et al. 1994; Dullo et al. 2009; Werner et al. 2016).

We provide single-shard electron microprobe and LA-ICP-MS data on all the samples and compare to available geochemical databases, which permits us to link the tephra layers in this study to three caldera complexes within the Aleutian arc. One of the tephras, labeled Br2, is the first discovery of ash from the well-known ~3.6 ka Aniakchak II caldera-forming eruption (Alaska) in Bering Sea sediments, which permits significant enlargement of its earlier known ashfall area. Tephra SR2 (~12.2 ka) likely belongs to the post-glacial caldera-forming eruption at Semisopochnoi Island (Western Aleutian Islands), and tephra SR4 (~64.5 ka) informs on an earlier unknown large eruption from Okmok (Umnak Island, Eastern Aleutian Islands).

## Materials and methodology

### Stratigraphy and ages of tephra layers

Stratigraphic position of the studied tephra layers relative to sedimentary units was determined based on the on-board descriptions of the cores (Fig. 2; Dullo et al. 2009; Gorbarenko et al. 2010). Age estimates used here are based on published age-depth models for the cores GC11, GC13, SO201-2-77 KL, SO201-2-81 KL, and SO201-2-85 KL (Gorbarenko et al. 2010; Max et al. 2012; Riethdorf et al. 2013; Malakhov and Gorbarenko, unpublished data) and stratigraphic data on the Bering Sea sediments (Gorbarenko and Artyomova 2003; Alekseeva et al. 2015). Early Holocene parts of these age models are based on radiocarbon dates (Gorbarenko et al. 2005; Max et al. 2012) and, following these authors, we provide our age estimates for the SR2 and V1.1 tephras in calibrated years before 1950 AD.

### Chemical analysis of volcanic glass and minerals

Samples were taken from well-defined visible tephra layers and wet-sieved to obtain 50–100 μm and > 100 μm fractions. Pumice lapilli were crushed, and the resulting coarse ash was sieved in the same way. Morphology of glass shards from ash layers was examined under a binocular microscope and described based on the classification of Katoh et al. (2000). The 50–100 μm fraction was further processed to obtain > 2.85 g/cm$^3$ fractions for the study of mafic mineral composition. Minerals were extracted from six samples and examined using a polarizing microscope (≥ 300 grains per sample) for identification and estimation of relative abundances. All the samples used in this study are listed in the Online Resource 1.

#### Electron microprobe analysis

Electron microprobe analysis (EMPA) of volcanic glass was performed on the > 100-μm fraction in 21 ash samples and in 3 samples of pumice lapilli. The resulting dataset comprises 327 analyses obtained during 8 probe sessions conducted between 2009 and 2014 at the GEOMAR Helmholtz Centre for Ocean Research Kiel, using a JEOL JXA 8200 electron microprobe. All analyses were performed under the same analytical conditions at a 15 kV accelerating voltage with a beam diameter of 5 μm and a beam current of 6 nA. A detailed account of analytical conditions, which includes internal standards and count times, was described in Ponomareva et al. (2017). For all comparisons, data were normalized to an anhydrous basis (i.e., 100% total oxides) and data with analytical totals below 94 wt.% were excluded. Normalized data, originally obtained raw data totals, and data on reference materials from each analytical session are provided in Online Resource 2. Average values for glass from each tephra sample and from each tephra are provided in Table 1.

Minerals were analyzed for six samples using the JEOL JXA 8200 electron microprobe at GEOMAR. Analyses were performed using a focused electron beam at 20 nA and 15 kV accelerating voltage and corrected using the CITZAF built-in JEOL software. The measurement time was 20 s on peak and 10 s on background, for all elements. Natural minerals (scapolite USNM R6600-1, pyroxene USNM 12214, hornblende USNM 111356, chromite USNM 117075, and ilmenite USNM 96189) (Jarosewich et al. 1980), as well as synthetic oxides, were used for calibration and checking of data quality. Representative compositions of minerals are given in Online Resource 3.

## LA-ICP-MS analysis

Trace element analyses of individual glass shards (Online Resource 4) were performed using laser ablation-inductively coupled plasma-mass spectrometry (LA-ICP-MS) at the Institute of Geosciences, Kiel University (Germany). The analyses were obtained on September 12, 2010, March 23–24, 2011, and May 5 and August 1, 2017, using a Coherent GeoLas ArF 193 nm Excimer LA system and a quadrupole-based (QP) ICP-MS Agilent 7500s in 2010–2011 and Agilent 7900 in 2017. A detailed description of the technique can be found in Ponomareva et al. (2013a) and Cook et al. (2018). Metadata concerning the instrumental conditions and other analytical details are provided in Online Resource 4. Data quality was checked

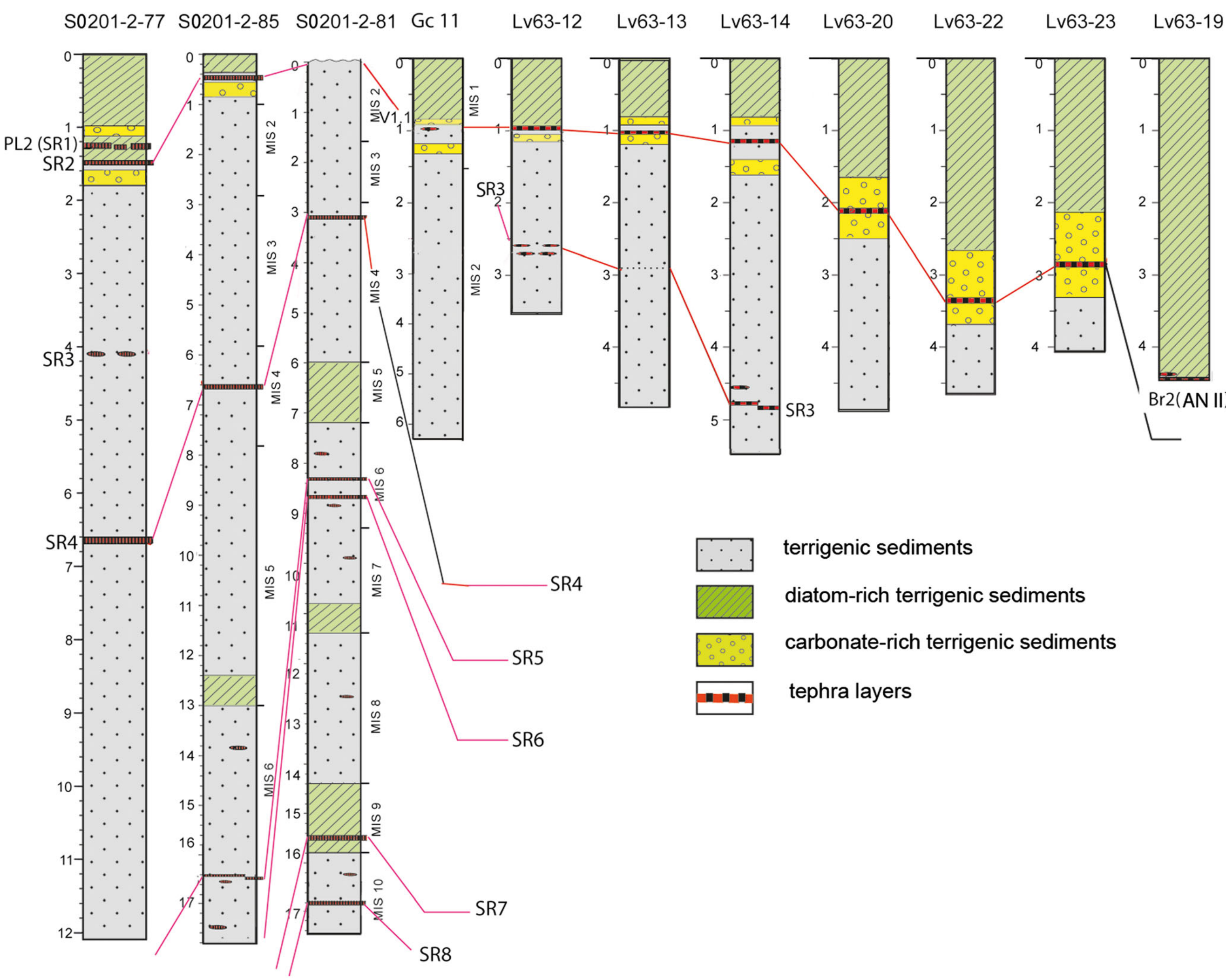


**Fig. 2** Schematic graphic presentation of marine sediment cores considered in this study. Tephra labels are given left and right of the cores. SR followed by a number is for the tephra layers first identified in the Shirshov Ridge cores: PL2 (SR1) ~ 10.2 ka, Plosky volcanic massif (Ponomareva et al. 2013b); SR2 ~ 12.2 ka, Semisopochnoi volcano (this study); SR4 ~ 64.5 ka, Okmok volcano (this study); SR6 (~ 177 ka Rauchua tephra)—presumably from the Karymsky eruptive center (Kamchatka); SR3, SR5, SR7, SR8—tephra from unknown sources. Br2 (CFE II)—tephra from the ~ 3.6 ka Aniakchak caldera-forming eruption (Alaska)

**Table 1** Average chemical composition of volcanic glass from tephra layers in the Bering Sea sediments

| Core ID | Interval (cm b.s.f.) | Tephra ID | $SiO_2$ | $TiO_2$ | $Al_2O_3$ | FeOt | MnO | MgO | CaO | $Na_2O$ | $K_2O$ | $P_2O_5$ | F | $SO_3$ | Cl | Total | *n* |
|---|---|---|---|---|---|---|---|---|---|---|---|---|---|---|---|---|---|
| Lv-63-19-1 | 440–448 | Br2 (rhy) average | 70.97 | 0.49 | 15.06 | 2.41 | 0.13 | 0.50 | 1.79 | 5.34 | 2.96 | 0.08 | 0.05 | 0.02 | 0.20 | 100.00 | 34 |
| | | | (0.42) | (0.04) | (0.18) | (0.26) | (0.09) | (0.05) | (0.09) | (0.28) | (0.11) | (0.04) | (0.08) | (0.03) | (0.02) | | |
| Lv-63-19-1 | 440–448 | Br2 (and) | 59.12 | 1.47 | 16.10 | 6.73 | 0.24 | 2.73 | 6.15 | 4.78 | 1.55 | 0.68 | 0.07 | 0.26 | 0.10 | 100.00 | 1 |
| SO201-2-77 | 116–117 | *SR2 (PL2) | 65.43 | 0.76 | 15.55 | 4.95 | 0.17 | 1.01 | 2.97 | 5.00 | 3.41 | 0.41 | 0.07 | 0.04 | 0.23 | 100.00 | 3 |
| | | | (1.75) | (0.04) | (0.14) | (0.78) | (0.04) | (0.41) | (0.57) | (0.38) | (0.19) | (0.10) | (0.06) | (0.01) | (0.04) | | |
| SO201-2-77 | 145 | SR2 | 65.66 | 0.73 | 15.68 | 4.75 | 0.18 | 0.97 | 2.89 | 5.27 | 3.32 | 0.28 | 0.00 | 0.04 | 0.24 | 100.00 | 19 |
| | | | (2.61) | (0.27) | (0.67) | (1.17) | (0.12) | (0.43) | (0.84) | (0.39) | (0.22) | (0.31) | (0.00) | (0.05) | (0.04) | | |
| SO201-2-79 MUC | 3–5 | SR2 | 65.14 | 0.77 | 15.91 | 4.86 | 0.15 | 1.07 | 3.24 | 4.98 | 3.24 | 0.34 | 0.06 | 0.02 | 0.21 | 100.00 | 12 |
| | | | (1.21) | (0.12) | (0.68) | (0.78) | (0.04) | (0.26) | (0.71) | (0.23) | (0.30) | (0.09) | (0.09) | (0.02) | (0.03) | | |
| SO201-2-81 MUC | 10–13 | *SR2 (PL2) | 64.93 | 0.80 | 15.61 | 4.99 | 0.14 | 1.22 | 3.26 | 5.20 | 3.19 | 0.34 | 0.06 | 0.04 | 0.21 | 100.00 | 4 |
| | | | (0.96) | (0.05) | (0.41) | (0.73) | (0.08) | (0.13) | (0.33) | (0.10) | (0.20) | (0.17) | (0.15) | (0.02) | (0.02) | | |
| SO201-2-81 MUC | 14–17 | *SR2 (PL2) | 64.46 | 0.80 | 15.77 | 5.18 | 0.19 | 1.18 | 3.37 | 5.21 | 3.20 | 0.32 | 0.08 | 0.03 | 0.21 | 100.00 | 6 |
| | | | (0.54) | (0.10) | (0.21) | (0.51) | (0.08) | (0.12) | (0.22) | (0.49) | (0.08) | (0.09) | (0.09) | (0.03) | (0.02) | | |
| SO201-2-85 | 47–55 | SR2 | 64.86 | 0.76 | 15.87 | 4.98 | 0.19 | 1.14 | 3.17 | 5.21 | 3.27 | 0.31 | 0.00 | 0.03 | 0.21 | 100.00 | 15 |
| | | | (3.28) | (0.25) | (0.42) | (1.53) | (0.09) | (0.59) | (1.02) | (0.31) | (0.44) | (0.26) | (0.00) | (0.03) | (0.03) | | |
| Lv63-12-1 | 91–93 | SR2 | 65.13 | 0.77 | 15.86 | 4.88 | 0.16 | 1.07 | 3.13 | 5.16 | 3.19 | 0.33 | 0.07 | 0.04 | 0.21 | 100.00 | 14 |
| | | | (1.58) | (0.12) | (0.73) | (0.80) | (0.09) | (0.28) | (0.61) | (0.37) | (0.38) | (0.13) | (0.09) | (0.04) | (0.06) | | |
| Lv63-14-1 | 118–121 | SR2 | 64.48 | 0.82 | 15.87 | 5.22 | 0.20 | 1.22 | 3.41 | 5.03 | 3.09 | 0.36 | 0.05 | 0.04 | 0.21 | 100.00 | 18 |
| | | | (2.09) | (0.13) | (0.73) | (0.92) | (0.08) | (0.45) | (0.94) | (0.32) | (0.53) | (0.14) | (0.08) | (0.04) | (0.04) | | |
| Lv63-20-2 | 210–212 | SR2 | 65.12 | 0.76 | 15.76 | 4.93 | 0.18 | 1.13 | 3.17 | 5.14 | 3.19 | 0.30 | 0.07 | 0.04 | 0.22 | 100.00 | 17 |
| | | | (1.82) | (0.13) | (0.32) | (0.79) | (0.07) | (0.32) | (0.59) | (0.27) | (0.21) | (0.13) | (0.11) | (0.04) | (0.04) | | |
| Lv63-23-2 | 282.5–284.5 | SR2 | 64.57 | 0.80 | 15.82 | 5.20 | 0.19 | 1.21 | 3.35 | 5.08 | 3.13 | 0.34 | 0.05 | 0.04 | 0.22 | 100.00 | 33 |
| | | | (2.63) | (0.20) | (0.58) | (1.03) | (0.09) | (0.56) | (1.02) | (0.38) | (0.43) | (0.24) | (0.09) | (0.05) | (0.07) | | |
| SR2 average | | SR2 | 64.93 | 0.78 | 15.80 | 5.01 | 0.18 | 1.13 | 3.21 | 5.13 | 3.20 | 0.32 | 0.05 | 0.04 | 0.22 | 100.00 | 141 |
| | | | (2.34) | (0.19) | (0.59) | (1.04) | (0.09) | (0.46) | (0.88) | (0.38) | (0.39) | (0.21) | (0.10) | (0.04) | (0.05) | | |
| GC11 | 95–97 | V1.1 | 64.41 | 0.79 | 15.85 | 5.38 | 0.19 | 1.13 | 3.39 | 5.01 | 3.21 | 0.36 | 0.05 | 0.02 | 0.21 | 100.00 | 13 |
| | | | (1.01) | (0.11) | (0.75) | (0.49) | (0.07) | (0.30) | (0.46) | (0.26) | (0.28) | (0.10) | (0.09) | (0.03) | (0.04) | | |
| SO201-2-77 | 650–654 | SR4 | 53.70 | 1.71 | 14.86 | 12.10 | 0.23 | 4.05 | 8.40 | 3.54 | 1.02 | 0.26 | 0.00 | 0.06 | 0.08 | 100.00 | 19 |
| | | | (1.25) | (0.30) | (1.28) | (1.59) | (0.10) | (0.38) | (0.74) | (0.81) | (0.19) | (0.06) | (0.00) | (0.08) | (0.02) | | |
| SO201-2-81 | 307–316 | SR4 | 53.72 | 1.74 | 15.04 | 11.88 | 0.23 | 4.03 | 8.42 | 3.47 | 1.01 | 0.33 | 0.00 | 0.05 | 0.07 | 100.00 | 55 |
| | | | (1.26) | (0.38) | (0.60) | (1.04) | (0.16) | (0.52) | (0.64) | (0.90) | (0.26) | (0.09) | (0.00) | (0.05) | (0.03) | | |
| SO201-2-85 | 660–665 | SR4 | 53.78 | 1.70 | 14.98 | 11.89 | 0.24 | 4.02 | 8.32 | 3.62 | 1.07 | 0.26 | 0.00 | 0.06 | 0.08 | 100.00 | 39 |
| | | | (1.30) | (0.31) | (1.04) | (1.23) | (0.08) | (0.53) | (0.68) | (0.69) | (0.26) | (0.08) | (0.00) | (0.09) | (0.02) | | |
| SR4 average | | | 53.74 | 1.72 | 14.99 | 11.92 | 0.23 | 4.03 | 8.38 | 3.53 | 1.03 | 0.29 | 0.00 | 0.06 | 0.08 | 100.00 | 113 |
| | | | (1.26) | (0.34) | (0.90) | (1.21) | (0.13) | (0.50) | (0.67) | (0.82) | (0.26) | (0.11) | (0.00) | (0.07) | (0.03) | | |

Note: *SR2 (PL2) glass shards admixed to the 10.2 ka PL2 tephra from the Plosky volcanic massif (Ponomareva et al. 2013a). "rhy" and "and" denote rhyolite and andesite glass populations in Br2 tephra. *b.s.f.* below sea floor. Values in parentheses are 2 standard deviations (2s). *n* number of analyses. To eliminate effects of secondary hydration and incomplete degassing on glass compositions, the concentrations were recalculated to 100 wt.% on anhydrous basis and averaged. Individual EMP glass analyses and original analytical totals are given in the Online Resource 2 using blind analysis of international reference glass BCR2-G, KL2-G, ATHO-G, and STHS60/8-G (Rocholl 1998; Jochum et al. 2006). The values recommended for these reference glass (Jochum and Nohl 2008) were typically reproduced within 5% for most elements conventionally measured by LA-ICP-MS (REEs, Zr, Nb, Ba, Y, Sr). Larger deviations are observed for less frequently determined elements, such as Li, B, As, and are likely related to some uncertainty in the reference values for these elements (Jochum et al. 2006). Average compositions for the major populations of glass from each tephra are provided in Table 2.

## Results

### Stratigraphy, age, and description of tephra layers

Tephra Br2 was found at the bottom of core Lv63-19, which is located at the northwest margin of the Aleutian Basin (Figs. 1 and 2). The stratigraphic position of the Br2 tephra within upper homogeneous diatom-rich terrigenic sediments indicates a mid-Holocene age (Gorbarenko et al. 2010). The tephra is composed of fine ash and forms 1–2-cm-thick lenses between depths of 440 and 450 cm below the sea floor. Glass shards from two different levels within this interval have

**Table 2** Mean trace element compositions of volcanic glass from tephra in Bering Sea sediments

| Tephra | Br2 | | SR2 | | SR4 | | Piip pumice | |
|---|---|---|---|---|---|---|---|---|
| | Mean (7) | *2s* | Mean (9) | *2s* | Mean (8) | *2s* | Mean (7) | *2s* |
| Li | 31.6 | *7.3* | 26.3 | *8.1* | 14.1 | *8.0* | 16.1 | *3.0* |
| Sc | 11.5 | *4.0* | 19.7 | *5.6* | 50.8 | *6.5* | 3.1 | *0.9* |
| Ti | 3152 | *1435* | 4694 | *1517* | 9421 | *1929* | 1123 | *168* |
| V | 3.3 | *1.7* | 50.7 | *73.4* | 439 | *93* | 3.6 | *0.6* |
| Rb | 68.5 | *8.1* | 85.3 | *36.9* | 26.8 | *22.2* | 15.5 | *1.6* |
| Sr | 196 | *24* | 280 | *137* | 359 | *32* | 84.4 | *4.4* |
| Y | 47.7 | *7.6* | 41.9 | *10.3* | 36.1 | *20.0* | 14.7 | *1.6* |
| Zr | 284 | *65* | 245 | *101* | 148 | *109* | 124 | *9* |
| Nb | 17.5 | *5.6* | 6.16 | *2.29* | 4.61 | *3.61* | 5.31 | *0.57* |
| Cs | 3.38 | *0.39* | 5.10 | *1.76* | – | – | 0.29 | *0.10* |
| Ba | 953 | *95* | 952 | *253* | 422 | *262* | 228 | *7* |
| La | 27.9 | *3.3* | 21.4 | *5.4* | 12.5 | *9.1* | 10.9 | *0.9* |
| Ce | 58.2 | *7.4* | 47.5 | *12.3* | 27.8 | *18.8* | 24.4 | *1.3* |
| Pr | 7.67 | *1.04* | 6.66 | *1.56* | 3.99 | *2.46* | 2.78 | *0.40* |
| Nd | 33.7 | *6.3* | 30.0 | *6.2* | 18.9 | *11.1* | 10.5 | *3.3* |
| Sm | 7.71 | *1.92* | 7.35 | *1.47* | 5.01 | *2.91* | 2.43 | *0.83* |
| Eu | 2.11 | *0.23* | 1.86 | *0.28* | 1.59 | *0.62* | 0.47 | *0.21* |
| Gd | 8.24 | *1.97* | 7.18 | *1.38* | 5.99 | *3.08* | 2.23 | *0.69* |
| Tb | 1.24 | *0.23* | 1.07 | *0.26* | 0.94 | *0.45* | 0.35 | *0.07* |
| Dy | 8.42 | *2.69* | 7.00 | *1.63* | 5.99 | *3.02* | 2.28 | *0.58* |
| Ho | 1.74 | *0.38* | 1.48 | *0.33* | 1.28 | *0.61* | 0.49 | *0.13* |
| Er | 5.29 | *1.05* | 4.61 | *1.20* | 3.95 | *2.15* | 1.53 | *0.29* |
| Tm | 0.76 | *0.14* | 0.67 | *0.19* | 0.54 | *0.26* | 0.28 | *0.07* |
| Yb | 5.41 | *0.99* | 4.61 | *1.29* | 3.70 | *1.96* | 1.76 | *0.36* |
| Lu | 0.82 | *0.14* | 0.71 | *0.21* | 0.56 | *0.28* | 0.28 | *0.07* |
| Hf | 7.35 | *0.92* | 6.28 | *2.46* | 3.91 | *2.54* | 3.48 | *0.61* |
| Ta | 1.10 | *0.18* | 0.36 | *0.14* | 0.31 | *0.22* | 0.41 | *0.07* |
| Pb | 19.2 | *15.7* | 18.3 | *5.4* | 11.4 | *6.8* | 5.19 | *0.66* |
| Th | 6.54 | *0.68* | 6.19 | *2.32* | 2.75 | *2.04* | 1.51 | *0.36* |
| U | 3.04 | *0.65* | 3.11 | *1.22* | 1.31 | *1.03* | 0.87 | *0.12* |

Note: Br2 composition calculated for rhyolite shards only. The number of analyses used to calculate the mean values is indicated in parentheses. 2s—two standard deviations. Complete set of data can be found in the Online Resource 4 identical morphologies and are dominated by colorless fibrous and bubble-wall stretched shards with subordinate amounts of platy shards. Light-brown shards of the same morphology are present in smaller amounts accompanied by rare brown shards with microlites. The heavy mineral assemblage for this tephra cannot be assessed due to a large admixture of terrigenic material.

Tephra SR2 was found in five piston and gravity cores (SO201-2-77 KL, SO201-2-85 KL, Lv63-12, Lv63-13, and Lv63-14) and two pilot cores (SO201-2-79 MUC and SO201-2-81 MUC) on the slopes of the Shirshov Ridge, as well as in three gravity cores at the northwestern margin of the Aleutian Basin (Lv63-20, Lv63-22, and Lv63-23; Fig. 1). Tephra SR2 varies in thickness from 1 to 4 cm and is represented by dark-gray fine ash with occasional ≤ 1 mm pumice grains. The tephra forms a distinct layer clearly identified against the greenish-gray sedimentary background due to its dark color and strong compaction. Because of the latter, the SR2 layer was deformed in most of the cores.

Tephra SR2 is stratigraphically positioned within Younger Dryas sediments (Max et al. 2012; Alekseeva et al. 2015). The age of the SR2 tephra can be estimated at ~ 12.2 ka based on close estimates of 12.14 and 12.29 ka for the bottom of the SR2 layer in the age models for the cores SO201-2-77 KL and SO201-2-85 KL, respectively (Max et al. 2012). Based on similar features and deformation, as well as on stratigraphic position, the SR2 tephra was likely recovered by adjacent core 18–6 from the R/V Sonne SO202 INOPEX (Innovative North Pacific Experiment) cruise (Gersonde 2012; Kuehn et al. 2014) as well as by cores taken during the R/V MIRAI cruise MR06-04 (Harada 2006) (Fig. 1).

Most of the SR2 glass are light gray with a brownish hue and have frothy morphologies. Dark-brown to dark-gray, frothy and bubble-wall stretched, or blocky, shards occur in smaller amounts, and brown rock fragments are rare. Many shards contain numerous small microlites of plagioclase, pyroxene, ore minerals, and rare apatite. The mafic mineral assemblage includes (in descending order of abundance) clino- and orthopyroxene, titanomagnetite, ilmenite, apatite, and hornblende (Online Resource 3). Clinopyroxene (augite with Mg# = 59–81 mol%, average 72 mol%) prevails over orthopyroxene (predominantly hypersthene with Mg# = 52–73 mol%, average 62 mol%). The Cpx/Opx ratio is ~ 3. All samples have admixed terrigenic grains of epidote, hematite, chlorite, actinolite, mica, rare garnet, zircon, and sphene. The abundance of terrigenic grains increases with height in the tephra layer.

Tephra V1.1 occurs in cores GC11 and GC13 at the western foot of the Bowers Ridge (in the southern part of the Aleutian Basin, Fig. 1) (Gorbarenko et al. 2010), and exhibits mineral and chemical compositions close to those in SR2. However, it has an age of ~ 10.5 ka (Gorbarenko and Artyomova 2003; Gorbarenko et al. 2010); younger by ~ 2 ka than SR2. In addition, it is composed of rounded coarse (up to 2 mm) pumice grains and glass-coated crystals with a high proportion of terrigenic rock fragments, suggesting that it has been redeposited from adjacent islands by sediment gravity currents.

Tephra SR4 was found in three cores (SO201-2-77 KL, SO201-2-81 KL, and SO201-2-85 KL) on the Shirshov Ridge (Figs. 1 and 2). It forms a 4–9-cm-thick black fine ash layer, partly deformed by coring. The age of SR4 is estimated at ~ 64.5 ka based on the age models for cores SO201-2-77 KL and SO201-2-85 KL (Riethdorf et al. 2013; Malakhov and Gorbarenko, unpublished data).

SR4 is dominated by dark-gray and black, frothy, glass shards, and light-brown fibrous and bubble-wall stretched glass shards. A characteristic feature of this tephra is the presence of abundant olivine microlites with Fo content ranging from 63.5 to 83 mol% (Online Resource 3). The prevailing olivine composition is $Fo_{70-72}$. The other mafic phases are high-Ca pyroxene (mostly augite, and rare diopside and salite with Mg# = 53–83 mol%, average 74 mol%) and Ti-magnetite. Hypersthene with Mg# = 53–65 mol% is present in subordinate amounts (Cpx/Opx = 5–6). Rare amphibole grains also occur but are likely terrigenic.

## Chemical composition of glass

Br2 tephra glass have predominantly homogeneous medium-K rhyolite compositions (Fig. 3a, b). A single analyzed shard has a trachyandesitic composition ($SiO_2$ = 59.1 wt.%, $K_2O$ + $Na_2O$ = 6.34 wt.%). Due to high FeO/MgO ratios, the glass are classified as predominantly Fe-rich (Arculus 2003) or tholeiitic (Miyashiro 1975) (Fig. 3c). The glass have trace element patterns typical of arc magmas (Gill 1981) and exhibit moderately high light rare earth element (REE) to middle REE ratios ($La_n/Sm_n$ = 1.9–2.9, where lower index *n* denotes the concentrations normalized to primitive mantle). Glass also show enrichment in Pb, Th, U, large ion lithophile elements (LILE, e.g., Ba, Rb, Cs) relative to light REE, Nb, and Ta (Fig. 4a). The rhyolite glass exhibit strong depletion in Sr and Ti. Concentrations of highly incompatible elements (left part of spectra from Cs to La), Zr and Hf in andesitic shard are 1.5–2 times lower than in rhyolites, middle and heavy REE are similar or c. 20% lower (Fig. 4a). Contents of Sr and Ti are 2.5 times higher in the trachyandesitic shard and show little fractionation from REE.

SR2 tephra glass have somewhat heterogeneous high-K and high-Fe trachydacite compositions ($SiO_2$ = 65–68 wt.%, $K_2O + Na_2O$ = 7.5–9 wt.%) (Fig. 3a, b). The compositions of SR2 tephra glass from disparate cores tightly overlap and match the composition of the coarse V1.1 pumice, described at the western foot of the Bowers Ridge, ~ 150 km from the nearest active volcanoes (Figs. 1 and 3; Table 1).

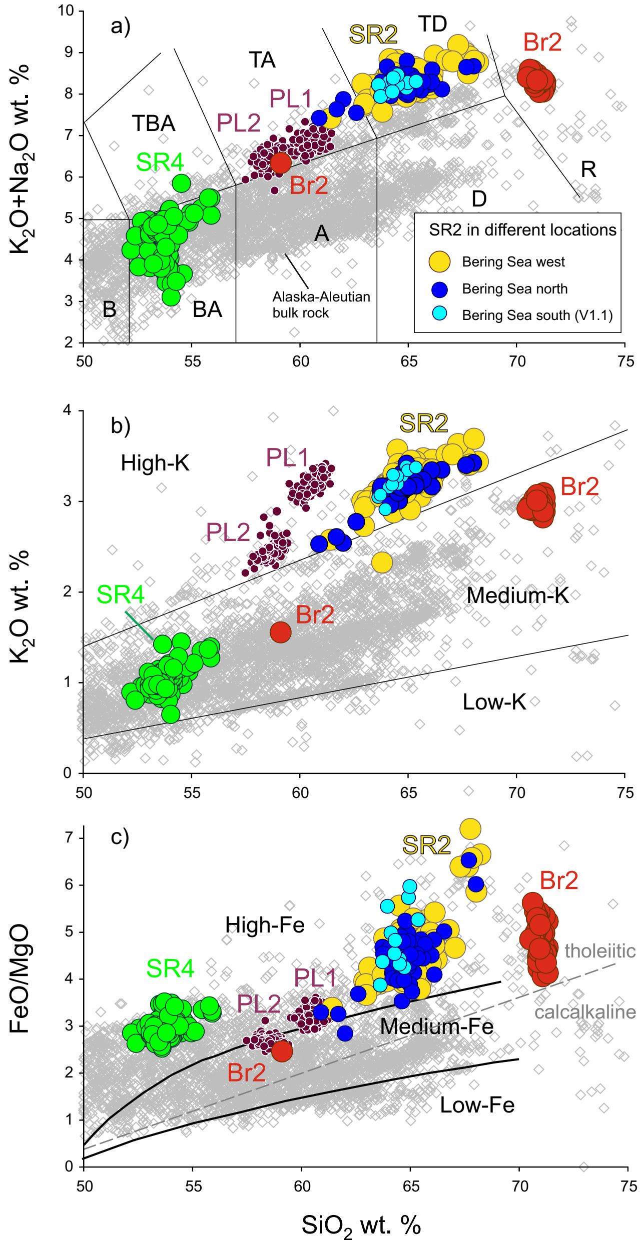


**Fig. 3** Classification diagrams for glass from tephra from the Bering Sea sediments compared to bulk rock data for the Alaska-Aleutian arc volcanoes. In the TAS diagram (**a**) fields are according to Le Bas et al. (1986): *B* basalt, *BA* basaltic andesite, *A* andesite, *D* dacite, *TB* trachybasalt, *BTA* basaltic trachyandesite, *TA* trachyandesite, *TD* trachydacite. In the $SiO_2$ vs $K_2O$ diagram (**b**), the fields of low-, medium-, and high-K rocks are according to Gill (1981). In the $SiO_2$ vs FeO/MgO diagram (**c**), tholeiitic and calc-alkaline series after Miyashiro (1975), and low-, medium-, and high-Fe series after Arculus (2003). FeO in bulk samples refers to total Fe expressed as FeO. For explanations of tephra labels see the text

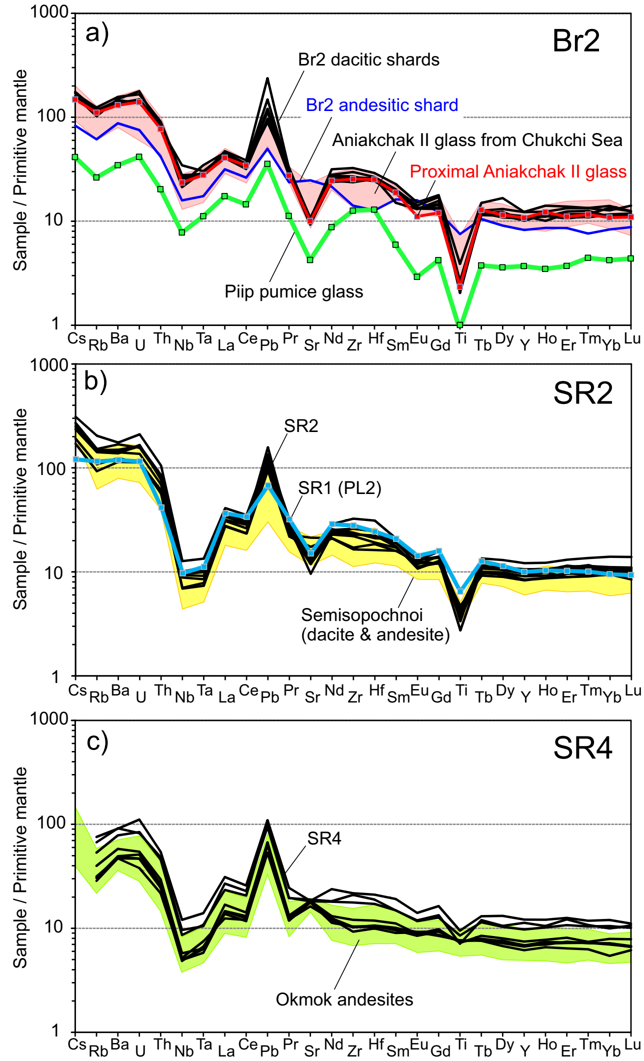


**Fig. 4** Trace element concentrations in single glass shards from studied tephras. **a** Br2 glass in comparison with the compositions of rhyolite glass from the proximal Aniakchak II deposits (Pearce et al. 2004), distal Aniakchak II glass from the Chukchi Sea sediments (Ponomareva et al. 2018), and average composition of glass from Piip volcano pumice (this study). **b** SR2 glass in comparison with an average composition of dacite and andesite from Semisopochnoi volcano (Delong et al. 1985) and PL2 (SR1) glass from Plosky volcano in Kamchatka (Ponomareva et al. 2013b). **c** SR4 glass in comparison with andesites and basaltic andesites from Okmok volcano (AVO geochemical database, Cameron et al. 2014; Nye et al. 2018). Normalization to primitive mantle (McDonough and Sun 1995)

The SR2 glass are compositionally close to those from the PL1 and PL2 tephras dated at ~11.6 and ~10.2 ka, respectively, from the Plosky volcanic massif in Kamchatka, Russia (Fig. 3; Ponomareva et al. 2013b). The PL2 tephra was found in many terrestrial sites in Kamchatka as well as in the cores SO201-2-77 KL (at 116–117 cm) and SO201-2-81 MUC (at 10–13 and 14–17 cm). In core SO201-2-77 KL, both PL2 and SR2 are present, and SR2 lies 26 cm lower than PL2. In other cores, only one of these tephras is present, so it is important to distinguish between them. The SR2 glass are distinguished from the Plosky glass by lower $TiO_2$ and $K_2O$, and generally higher silica content (Fig. 3). Trace element patterns of SR2 glass are typical of arc types (Gill 1981), with moderate light REE enrichment ($La_n/Sm_n$ = 1.7–2.0) and strong enrichments in Pb, LILE, Th, and U (Fig. 4b). The SR2 patterns are similar to PL2 glass for most elements from Nb through Lu, but show a stronger depletion in Ti and enrichment in Pb. The two tephras are best distinguished in the left part of the trace element spectra (Fig. 4b). SR2 glass are more enriched in highly incompatible elements U, Th, Ba, and Cs, and have higher Th/Nb, U/Nb, and Ba/Nb ratios.

SR4 glass have a distinct medium-K, high-Fe basaltic andesite composition (Fig. 3). Together with abundant olivine and pyroxene crystals, this suggests a basaltic bulk composition. Trace element concentrations in single glass shards vary by factor of ~ 2 (1.7–2.9) and are mostly parallel to each other except for Sr and Ti (Fig. 4c), which vary only slightly, by a factor of 1.2–1.3. The trace element variations suggest variable extents of crystal fractionation from a common parental melt in the presence of plagioclase and magnetite along with olivine and pyroxene (Fig. 4c). The glass exhibit typical arc-type patterns (Gill 1981), with monotonous enrichment from heavy REE to light REE ($La_n/Sm_n$ = 1.4–1.8, $Sm_n/Yb_n$ = 1.4–1.7), well pronounced Nb-Ta minima ($La_n/Nb_n$ = 2.4–3.0), and enrichment in Pb, LILE, Th, and U. Relative Sr enrichment ($Sr_n/Ce_n > 1$) is observed in the most primitive glass, which also have the lowest concentrations of other incompatible trace elements.

## Discussion

### Identification of source volcanoes

The tephra layers described in our study have well-expressed island-arc geochemical signatures (Gill 1981). They cannot have been derived from St. Paul Island or any other monogenetic basaltic lava field along the eastern Bering Sea margin (Wood and Kienle 1990), as these all have intra-plate geochemical characteristics (Moll-Stalcup 1994; Wirth et al. 2002). The tephras under consideration, however, could have originated from both the Kamchatka and Aleutian arcs bordering the Bering Sea from west and south, respectively (Fig. 1). The Kamchatkan sources are particularly plausible as our Bering Sea tephra sites are located downwind from the Kamchatka volcanoes. However, the Br2, SR2, or SR4 tephra layers have not been identified in any cores taken closer to Kamchatka (Dullo et al. 2009; Derkachev et al. 2015). Further, neither these nor compositionally similar tephras are known from the extensively sampled Kamchatka mainland (Braitseva et al. 1997; Kyle et al. 2011; Plunkett et al. 2015; Ponomareva et al. 2013a, 2015b, 2017). Due to these reasons, we suggest that the source volcanoes for the three tephras considered here are likely located within the Aleutian arc.

The submarine Piip volcano lies at the westernmost terminus of the Aleutian arc and is the closest volcano to the cores taken on the Shirshov Ridge (Fig. 1). Piip's edifice is covered with pumice bombs and lapilli that originate from a summit eruption of likely Late Pleistocene-Holocene age (Werner et al. 2016). However, glass from Piip pumice have higher silica content (> 77 wt.%) and trace element compositions that differ from the compositions of glass of the tephra layers under consideration (Figs. 4a and 5). Thus, the source volcanoes for these tephras should be located further east in the Aleutian arc, or perhaps on mainland Alaska.

A widely adopted approach for correlation of tephra layers and identification of their sources is based on comparison of glass composition (e.g., Alloway et al. 2005; Lowe et al. 2017; Davies 2015). However, glass composition data are available only for some of the Alaska-Aleutian volcanoes (e.g., Bindeman et al. 2001; Carson et al. 2002; Coombs et al. 2018; Wallace et al. 2017), so that an arc-wide comparison of glass compositions is impossible.

To narrow down our search for possible source volcanoes, we used another approach based on the comparison of glass and bulk rock compositions. Direct comparison of absolute concentrations of elements in glass and bulk rock analyses is compromised by the presence of variable amounts of mineral phenocrysts and accessory phases in bulk rocks. These host not only major rock forming elements, but can also selectively concentrate some trace elements, such as Sr in plagioclase, heavy REE in hornblende, REE in apatite. To eliminate this uncertainty, we used ratios of the most incompatible elements in both rocks and glass. Due to low mineral-melt partition coefficients ($D < 0.01$), the ratios of these elements remain nearly constant during mineral crystallization or accumulation in bulk magmas (e.g., Pearce and Parkinson 1993; Elliott et al. 1997; Kelemen et al. 2003a). These elements are placed on the left side of mantle-normalized diagrams and include La, Nb, Ta, Th, U, Ba, Rb, and Cs (Fig. 4). Of these elements, La, Nb, Ta, Th, and Ba are particularly useful because they are usually precisely defined in published datasets obtained through either INAA (Kay and Kay 1994) or, more recently, by ICP-MS (Cameron et al. 2014; Coombs et al. 2018; Nye et al. 2018). These elements are also relatively immobile during post-magmatic alteration, which can be an important effect of the presence of seawater and which easily disturbs concentrations of monovalent alkalis (Na, K, Rb, Cs) and U (Hart and Staudigel 1982).

In order to search for potential sources of our Bering Sea tephras, we compiled data for the Alaska-Aleutian volcanoes from the open access databases from the Alaska Volcano Observatory (Cameron et al. 2014; Coombs et al. 2018; Nye et al. 2018) and GEOROC n.d. (http://georoc.mpch-mainz.gwdg.de/georoc/). Some additional data have been included by courtesy of Gene Yogodzinski (University of South Caroline) from his compilation used in the review by Kelemen et al. (2003b) and as updated by Yogodzinski et al. (2015). We use these data to calculate incompatible trace element ratios for volcanic centers, which host calderas and large

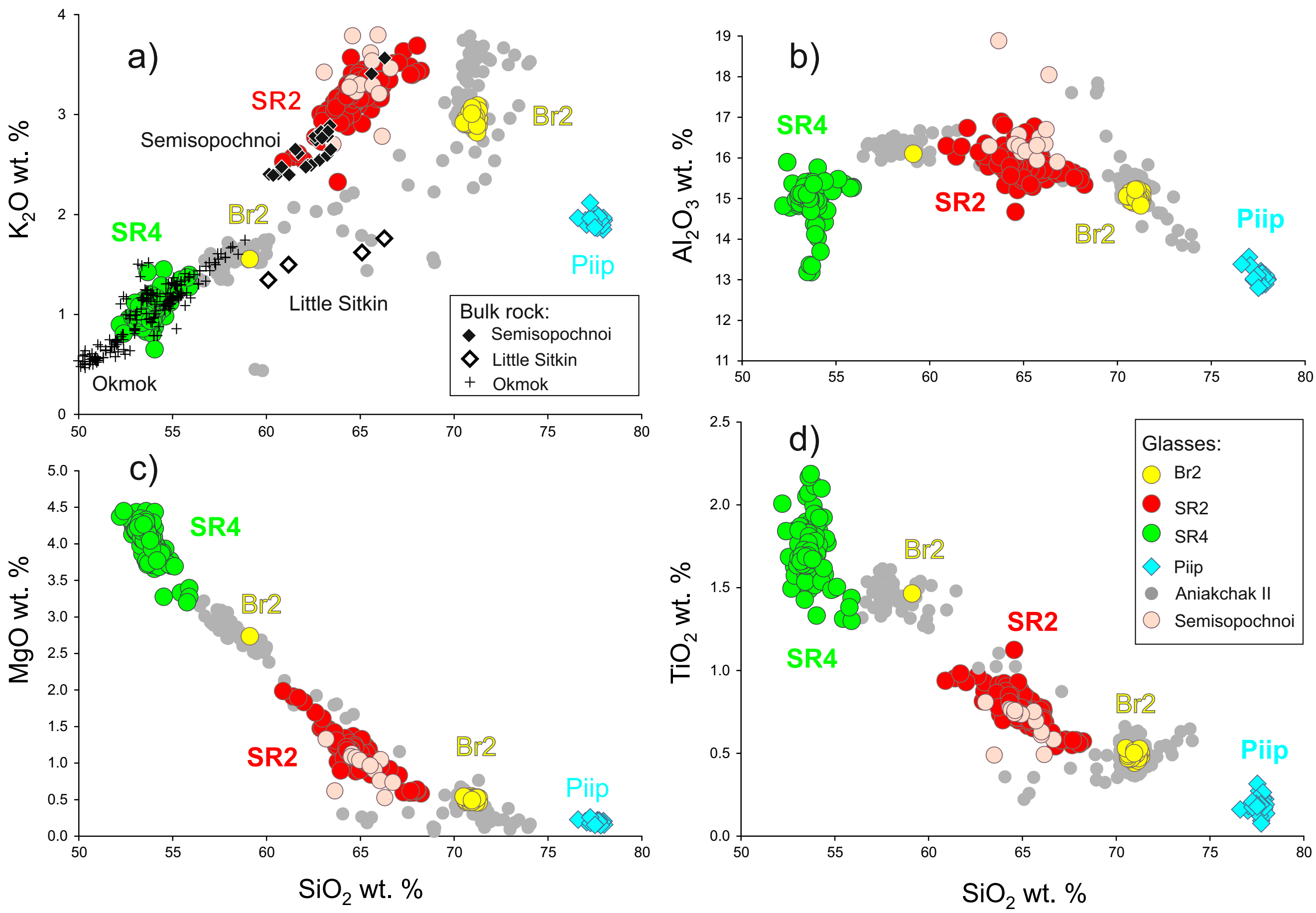


**Fig. 5** Comparison of glass data on Br2, SR2, and SR4 tephras with glass from Aniakchak (Wallace et al. 2017) and Semisopochnoi (Coombs et al. 2018), and with whole rock data from Little Sitkin, Semisopochnoi, and Okmok volcanoes (Cameron et al. 2014; Nye et al. 2018)

(> 2 km in diameter) craters. These data are shown in Figs. 6 and 7, and in Table 3. From Figs. 6 and 7, we can see that the large variability in source composition at Aleutian and Alaskan volcanoes permits a reliable identification or verification of the potential sources of the studied tephra layers.

## Tephra Br2

The Br2 tephra can be identified as a product of the Aniakchak volcanic center based on it having the lowest Ba/Nb, Th/Nb, La/Nb, along with moderately high Th/La, ratios in both bulk rock and glass chemistry data (Figs. 6 and 7). Comparison of all trace element concentrations with published Aniakchak II glass data (Pearce et al. 2004; Ponomareva et al. 2018) further confirms this conclusion (Fig. 4a).

Glass from the Br2 tephra have medium-K rhyolitic compositions and are geochemically similar to the rhyolitic population of the ~ 3.6 ka Aniakchak II glass (Kaufman et al. 2012; Davies et al. 2016; Wallace et al. 2017) (Figs. 5, 6, and 7). Only one of the analyzed Br2 shards falls into the andesitic Aniakchak II field; however, non-analyzed brown shards described in the samples likely indicate the presence of the whole andesite Aniakchak II population. Moreover, rhyolite Br2 glass are identical in composition to rhyolite glass from both proximal and ultra-distal (Chukchi Sea) Aniakchak II tephras. A single andesitic glass shard analyzed by LA-ICP-MS has a very similar trace element composition to that of andesitic Aniakchak II shards from Chukchi Sea sediments (Fig. 4a).

In comparison with rhyolitic glass from Piip pumice, Br2 glass are less siliceous and more enriched in alkalis (Fig. 5). A distinctive feature of both Br2 and Piip glass is a very modest depletion compared to average arc rocks in Nb and Ta relative to La and LILE (Fig. 4a). That is, there is a $La_n/Nb_n$ ratio of 1.2–2.1 in Br2 compared with 3.3 for the average Aleutian andesite (Kelemen et al. 2003b). The trace element pattern of Br2 glass is generally subparallel to that of Piip glass, except that there is a less pronounced Zr-Hf enrichment relative to middle REE in the latter. However, absolute trace element concentrations in Br2 glass are higher by a factor of 4–5 than for those of the Piip glass, thus precluding a genetic relationship.

Based on chemical similarity of Br2 glass to those from the 3.6 ka Aniakchak II tephra, its Holocene age (Fig. 2), and the

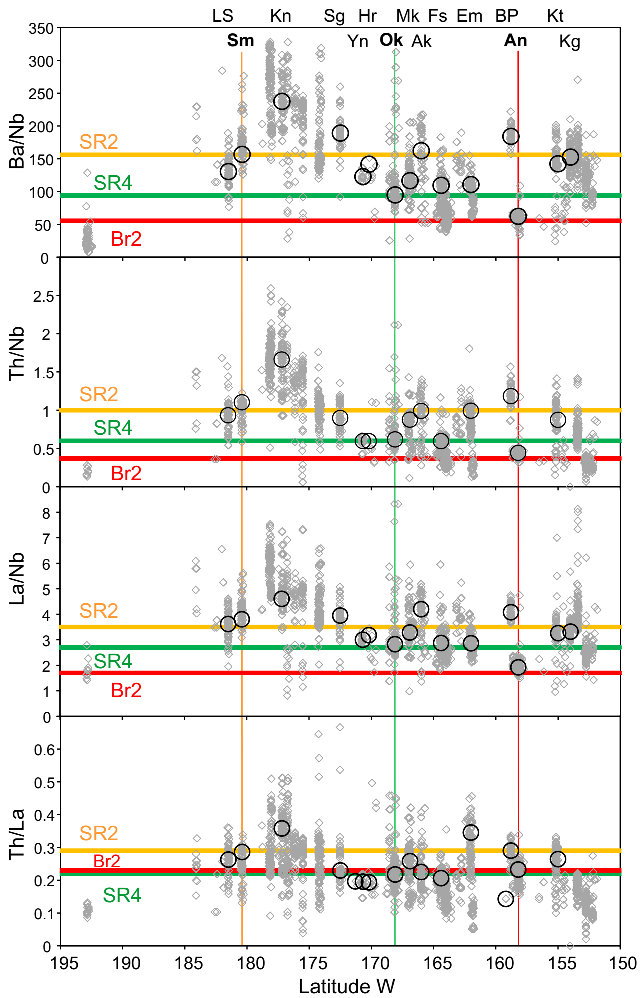


**Fig. 6** Along-arc variations of incompatible trace element ratios in bulk rocks from Alaska and Aleutians. Average compositions of glass from Br2, SR2, and SR4 tephra layers are shown by horizontal lines. Large circles show average composition of rocks for large caldera complexes and volcanoes with a large (> 2 km in diameter) crater (Table 3): *LS* Little Sitkin, *Sm* Semisopochnoi, *Kn* Kanaga, *Sg* Seguam, *Yn* Yunaska, *Hr* Herbert, *Ok* Okmok, *Mk* Makushin, *Ak* Akutan, *Fs* Fisher, *Em* Emmons Lakes, *BP* Black Peak, *An* Aniakchak, *Kt* Katmai, *Kg* Kaguyak

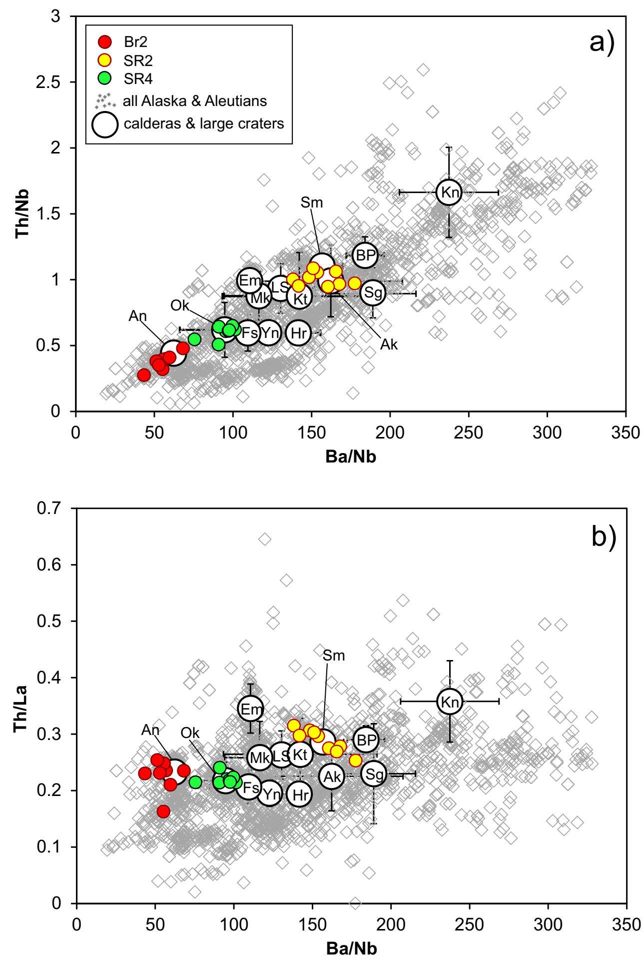


**Fig. 7** Variations in incompatible trace element ratios for single glass shards from tephra layers from Bering Sea, and in Alaska and Aleutian rocks. Large circles show average composition of rocks for large caldera complexes and volcanoes with a large (> 2 km in diameter) crater (Table 3). Abbreviations of calderas are given in the caption to Fig. 6. Error bars correspond to 1 standard deviation

aerial distribution of the Aniakchak II fall deposit (Davies et al. 2016; Graham et al. 2016; Pearce et al. 2017; Ponomareva et al. 2018), we suggest that the Br2 tephra correlates to the ~3.6 ka Aniakchak II eruption. A preliminary report on this finding by Derkachev et al. (2015) permitted Ponomareva et al. (2018) to use this site to develop a new isopach map for the Aniakchak II tephra fall deposit. The new map allows us to double the volume of this eruption from the value of 50 km$^3$ given by Miller and Smith (1987) to ~100 km$^3$. Assuming an ash density of 0.6 g/cm$^3$ (Kutterolf et al. 2008b) and rhyolite density of 2.6 g/cm$^3$, the dense rock equivalent (DRE) volume of the Aniakchak II tephra fall deposit is here estimated to be 23 km$^3$, with an erupted mass of $6.0 \times 10^4$ Mt. This corresponds to an eruption magnitude (M) of 6.8 (Pyle 1995; Mason et al. 2004).

Wide dispersal of the ~3.6 ka Aniakchak II tephra across the Bering Sea (Derkachev et al. 2015; Graham et al. 2016) permits significant enlargement of its known dispersal area (Davies et al. 2016) and indicates that it could also occur in northeast Asia (Fig. 1). The Aniakchak II tephra can also serve as a major Holocene marker horizon for the Bering Sea shelf, directly linking its Holocene sedimentary archives to those from the Chukchi Sea (Pearce et al. 2017; Ponomareva et al. 2018), eastern Canada (Pyne-O'Donnell et al. 2012), and Greenland (Pearce et al. 2004; Coulter et al. 2012; Jennings et al. 2014).

## Tephra SR2

The ~12.2 ka SR2 tephra forms a visible layer in the sediments on the Shirshov Ridge and at the northeastern margin of the Aleutian basin (Figs. 1, 2, and 3). Its thickness varies from 2 to 4 cm. In terms of incompatible trace element ratios (Figs.

**Table 3** Incompatible trace element characteristics of the Aleutian arc calderas and ash layers from the Bering Sea

| Name | *N* | Long (W) | Ba/Nb | *1s* | La/Nb | *1s* | Th/La | *1s* | Th/Nb | *1s* |
|---|---|---|---|---|---|---|---|---|---|---|
| Little Sitkin | 14 | 181.5 | 132 | *24* | 3.62 | *0.64* | 0.26 | *0.04* | 0.93 | *0.19* |
| Semisopochnoi[a] | 39 | 180.4 | 162 | *16* | 3.92 | *0.35* | 0.28 | *0.03* | 1.10 | *0.08* |
| Kanaga | 47 | 177.2 | 237 | *31* | 4.60 | *0.66* | 0.36 | *0.07* | 1.66 | *0.34* |
| Seguam | 46 | 172.5 | 189 | *27* | 3.95 | *0.59* | 0.23 | *0.09* | 0.90 | *0.19* |
| Amukta | No data | 171.3 | | | | | 0.20 | | | |
| Yunaska | 15 | 170.7 | 123 | *7* | 3.00 | *0.12* | 0.20 | *0.02* | 0.60 | *0.07* |
| Herbert | 2 | 170.2 | 142 | *14* | 3.18 | *0.36* | 0.19 | *0.01* | 0.60 | *0.01* |
| Mount Okmok | 180 | 168.1 | 95 | *29* | 2.83 | *0.81* | 0.22 | *0.03* | 0.62 | *0.21* |
| Makushin | 205 | 166.9 | 116 | *22* | 3.29 | *0.60* | 0.26 | *0.06* | 0.88 | *0.18* |
| Akutan | 95 | 166.0 | 162 | *45* | 4.20 | *0.91* | 0.23 | *0.06* | 0.99 | *0.27* |
| Fisher | 115 | 164.4 | 109 | *25* | 2.87 | *0.62* | 0.21 | *0.03* | 0.60 | *0.14* |
| Emmons Lake | 48 | 162.0 | 111 | *4* | 2.86 | *0.24* | 0.35 | *0.04* | 0.99 | *0.09* |
| Veniaminof | 2 | 159.4 | | | | | 0.14 | *0.00* | | |
| Black Peak | 44 | 158.8 | 184 | *12* | 4.08 | *0.27* | 0.29 | *0.02* | 1.18 | *0.14* |
| Peak Aniakchak | 290 | 158.2 | 62 | *7* | 1.92 | *0.26* | 0.23 | *0.02* | 0.44 | *0.06* |
| Ugashik | No data | 156.4 | | | | | | | | |
| Katmai | 55 | 155.0 | 142 | *49* | 3.26 | *1.02* | 0.26 | *0.06* | 0.87 | *0.33* |
| Kaguyak | 118 | 154.0 | 152 | *18* | 3.32 | *0.35* | | | | |
| Br2 | 7 | | 55 | *7* | 1.68 | *0.29* | 0.23 | *0.03* | 0.37 | *0.06* |
| SR2 | 8 | | 156 | *13* | 3.50 | *0.26* | 0.29 | *0.02* | 1.01 | *0.05* |
| SR4 | 9 | | 94 | *8* | 2.73 | *0.19* | 0.22 | *0.01* | 0.60 | *0.05* |

[a] Average for Semisopochnoi dacite and andesite

6 and 7), SR2 glass have compositions that plot in the typical range of the Aleutian rocks. Similar Ba/Nb, Th/Nb, and Th/La ratios are observed in rocks from a number of volcanoes along the entire Aleutian Arc (Little Sitkin, Semisopochnoi, Seguam, Akutan, Katmai) (Figs. 6 and 7). Thus, the trace elements do not allow unique identification of the source volcano for this layer. However, the composition of SR2 glass is very close to that of the redeposited V1.1 coarse pumice in cores GC11 and GC13 at the foot of the Bowers Ridge, which points to Little Sitkin and Semisopochnoi volcanoes in the Western Aleutian Arc as the most probable sources. Of these two volcanoes, Semisopochnoi appears to be the most likely source of the SR2 tephra glass. Both SR2 glass and andesite and dacite from Semisopochnoi volcano have overlapping and unusually high $K_2O$ contents, in comparison with other Aleutian volcanoes (Fig. 3a). Dacite of Little Sitkin has significantly lower $K_2O$ contents in comparison with SR2 glass (Fig. 5a). The correlation of SR2 to Semisopochnoi is further confirmed by the comparison of an extended range of trace elements in SR2 glass and Semisopochnoi andesite and dacite (Fig. 4b), as well as by comparison of SR2 glass to those in Semisopochnoi proximal pumice (Fig. 5, Coombs et al. 2018). The mineral assemblage of SR2 tephra (plagioclase, hypersthene, augite, magnetite, apatite) also fits the modal mineral composition of Semisopochnoi dacite and andesite (Delong et al. 1985).

Semisopochnoi is the largest historically active volcano in the central and western Aleutian arc with its most recent eruption having been in 1987 (Reeder 1990). The volcano hosts a 7 × 6 km post-glacial caldera (Wood and Kienle 1990). Ignimbrite from the caldera-forming eruption blankets much of Semisopochnoi Island and crops out along the coastal cliffs (Coombs et al. 2018).

The compositions of SR2 glass have slightly different, but systematically variable, trace element ratios. For example, Ba/Nb (138–178) in SR2 glass correlates inversely with Th/La (0.25–0.31), and positively with La/Nb (3.2–4.0) (Fig. 8). Similar correlations are also observed for Semisopochnoi bulk rock analyses, so that Ba/Nb and La/Nb ratios decrease from basalts to andesites; and Th/La increases. SR2 glass have compositions similar to Semisopochnoi andesites and dacites, but not to Semisopochnoi basalts and basaltic andesites. These variations are not expected from closed system fractional crystallization and instead suggest either mixing of two contrasting magma compositions or assimilation-fractional crystallization (AFC), and can be considered a characteristic feature of this volcano (Delong et al. 1985; Coombs et al. 2018). Incompatible trace element ratios in SR2 glass overlap with those in Semisopochnoi dacite and andesite (Coombs et al. 2018) (Fig. 8).

The extent and volume of the SR2 tephra, and consequently the magnitude of the parent eruption, can now be

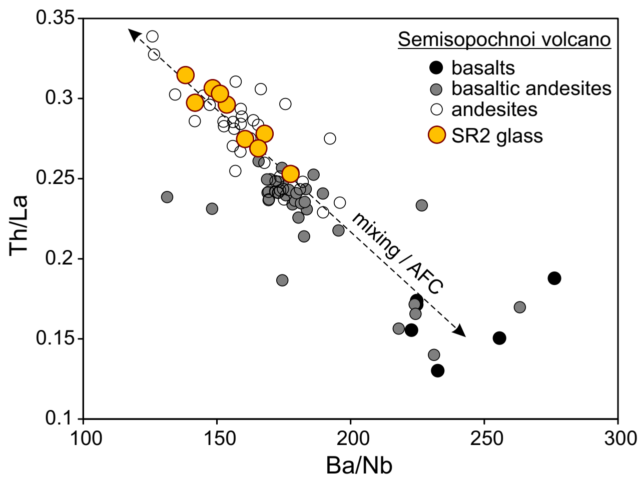


**Fig. 8** Variations of incompatible trace element ratios in Semisopochnoi rocks and SR2 glass. Whole rock data is after Delong et al. (1985) and Coombs et al. (2018). The variations are inconsistent with simple crystal fractionation from basalt to dacite magma and imply mixing of magmas from two different sources or assimilation of pre-existing crust. SR2 glass plot along the whole rock trend and correspond in composition to Semisopochnoi dacites and andesites

preliminary constrained from these data. The dispersal axis was directed NNW from the source (Fig. 1). Based on the known thicknesses of the SR2 tephra in all studied cores, we can here draft a preliminary tephra dispersal area (Fig. 1; Online Resource 5). The sites on the Shirshov Ridge are located close to each other and have a median tephra thickness of 3 cm. These sites, together with sites Lv63-30, -22, and -23 located at the northeastern margin of the Aleutian basin (Fig. 1), permit us to delineate a 2-cm isopach as a minimum concave line bounding all of these sites. The area within the 2-cm isopach is 767,400 km$^2$, so that—by applying the single-isopach approach (Legros 2000)—we obtain a minimum ashfall volume of 54 km$^3$. This corresponds to a volcanic explosivity index (VEI) six (Newhall and Self 1982). Assuming an ash density of 0.6 g/cm$^3$ (Kutterolf et al. 2008b), we obtain SR2 tephra mass of $3.2 \times 10^4$ Mt, and a DRE volume of 12 km$^3$. This corresponds to an eruption magnitude 6.5 (Pyle 1995; Mason et al. 2004). These are minimal estimates as they are based on only a few thickness measurements for SR2 tephra, and our calculations do not include the volume of the caldera fill or of ignimbrite dispersed beyond the caldera.

Based on the estimated size and geochemical similarity to the Semisopochnoi ignimbrite, we suggest that the SR2 tephra was a product of the caldera-forming eruption. Our age estimate of ~ 12.2 ka, as well as the stratigraphic position of the SR2 tephra within the Younger Dryas sediments, do not agree with a preliminary age estimate of 7.7–7.8 ka suggested by Coombs et al. (2018) for this ignimbrite. This discrepancy needs further investigation. At the same time, we do not observe any younger tephra of SR2 (and ignimbrite) composition in any of our cores. As a result, two closely spaced different and large eruptions from Semisopochnoi seem unlikely. The SR2 tephra is widely dispersed in the Aleutian basin, and can serve as a marker for the Younger Dryas climate interval.

## Tephra SR4

The ~ 64.5 ka SR4 tephra has a distinct basaltic andesite glass composition and was found in three cores on the Shirshov Ridge (Fig. 1). Comparison of our glass data with that of the Alaska Volcano Observatory Geochemical Database of whole rock compositions (Cameron et al. 2014; Nye et al. 2018) shows that SR4 glass compositions are very similar to basaltic andesites of Okmok volcano (Umnak Island, Eastern Aleutians) (Figs. 6 and 7). Additional support for this correlation comes from the discovery of a geochemically similar, but significantly younger (~ 12 ka), tephra in core U1343 at the eastern margin of the Aleutian basin, which is closer to Okmok (Fig. 1; Aoki et al. 2012). Peculiar features of Okmok rocks include predominantly mafic compositions, a common presence of olivine in the mineral assemblages, and relatively low Ba/Nb and La/Nb ratios (Figs. 6 and 7).

Okmok volcano last erupted in 2008 (Neal et al. 2009). The edifice hosts two overlapping calderas dated at ~ 12 and 2 ka; the younger caldera is about 9.5 km in diameter (Miller and Smith 1987; Larsen et al. 2007). Fall deposits and ignimbrites of the two known caldera-forming eruptions have mostly basaltic to intermediate bulk compositions with only a minor amount of more evolved material (Larsen et al. 2007). As the products of the volcano demonstrate similar compositions during its history (Finney et al. 2008; Larsen et al. 2013), it is possible that the ~ 64.5 SR4 tephra was also a product of Okmok.

The SR4 tephra forms a visible 4–5-cm-thick layer in three cores on the Shirshov Ridge. If the source of SR4 is Okmok volcano, then only justified isopach of 4 cm is an NW-SE elongated ellipse. This isopach embraces an area of 487,400 km$^2$. Accordingly, the single-isopach approach (Legros 2000) yields a minimum ashfall volume of 72 km$^3$, which corresponds to VEI 6 (Newhall and Self 1982). Adopting a density for basaltic ash of 0.8 g/cm$^3$ (Kutterolf et al. 2008b), and a basalt density of 3.0 g/cm$^3$, we obtain a total tephra mass of $5.8 \times 10^4$ Mt and DRE volume of 19 km$^3$, which corresponds to an eruption magnitude of 6.8 (Pyle 1995; Mason et al. 2004). These are only minimum estimates of the eruption parameters, as only few thickness measurements are available and no proximal deposits are known.

In the absence of well-documented proximal deposits, detailed reconstruction of possible mechanisms of this large eruption is not possible. The estimated volume of SR4 tephra of 20 km$^3$ DRE is, however, comparable to caldera-forming eruptions of Okmok that occurred over the past 12 ka and produced 30 $km^3$ (Okmok I) and 15 $km^3$ (Okmok II) DRE of basaltic material (Larsen et al. 2007). Both the Okmok I and Okmok II eruptions involved phreatomagmatic components. Larsen et al. (2007) thus concluded that interaction of magma with surface water and ice may trigger catastrophic eruptions of mafic magma at Okmok caldera, in addition to large amount of magmatic volatiles accumulated in magma chamber prior to the eruption. We suggest that the mid-Pleistocene Okmok eruption, which provisionally produced SR4 tephra, had a genesis similar to such recent eruptions. Because this older eruption occurred during the last glaciation, an interaction of voluminous basaltic magma with a thick ice cap in Okmok caldera is a plausible mechanism to facilitate the high explosivity of this eruption (Larsen et al. 2007).

## Conclusions

We describe three ash layers, labeled as Br2, SR2, and SR4, in the Bering Sea sediments. These are related to large explosive eruptions of Aleutian and Alaskan volcanoes over the last ~ 70 ka. These tephra layers are distinguished using major and trace element glass composition. To correlate with potential source volcanoes, we compared our glass analyses with whole rock compositions of the Alaska-Aleutian volcanoes. On this basis, we propose that the ratios of highly incompatible elements in whole rock analyses of rock samples (Ba/Nb, Th/La, Th/Nb, Nb/La) can be used to correlate their compositions with tephra glass compositions.

The Br2 tephra layer from the Beringian shelf comprises glass of rhyolite (dominant) and andesite (minor) medium-K composition and geochemically correlates with tephra from the ~ 3.6 ka Aniakchak II caldera-forming eruption (Alaska). This discovery allows us to increase the estimate of the Aniakchak II tephra volume to ~ 100 $km^3$ (DRE = 23 $km^3$). This doubles the previously published volume (Miller and Smith 1987) and increases the eruption magnitude to 6.8. The Aniakchak II tephra can serve as a major Holocene marker horizon for the Bering Sea shelf, directly linking its Holocene sedimentary archives to those from the Chukchi Sea, Canada, and Greenland (Pearce et al. 2004; Coulter et al. 2012; Pyne-O'Donnell et al. 2012; Jennings et al. 2014; Pearce et al. 2017; Ponomareva et al. 2018).

The SR2 tephra, with a peculiarly high-K trachydacitic composition, has an age of 12.2 ka and is geochemically correlated to volcanic products of the Semisopochnoi volcano in the Western Aleutian Arc. Ashfall from this eruption was dispersed to the northwest and covered an area of 767,400 $km^2$ with a 2-cm layer yielding a minimum ashfall volume of 54 $km^3$ (DRE = 12 $km^3$). This corresponds to an eruption magnitude of 6.5. The SR2 tephra is widely dispersed in Aleutian basin sediments, and can thus serve as a sensitive marker for the Younger Dryas climate interval.

The SR4 tephra, with an age of 64.5 ka, has a mafic composition. It contains abundant olivine and is geochemically correlated to Okmok volcano. The only justified isopach of 4 cm for this tephra is an NW-SE elongated ellipse, and this gives an area of 487,400 $km^2$, for a minimum ashfall volume of 72 $km^3$ (DRE = 19 $km^3$). This corresponds to an eruption magnitude of 6.8.

Our data suggest that Bering Sea sediments preserve a record of very large explosive eruptions of Alaska-Aleutian arc volcanoes. Some of these eruptions are unknown from proximal records due to erosion or burial by younger sediments. Detailed studies of the Bering Sea IODP sedimentary cores will undoubtedly discover further large eruptions, and this will become a part of an effort aimed at the reconstruction of the volcanic arc history, as well as its relation to paleoclimate. The widespread tephra layers also serve as useful isochrones allowing correlations of paleoclimate records across continents and neighboring seas.

**Acknowledgements** The tephra samples were obtained during cruises: (i) SO201-2 KALMAR (grant # 03G0672A and B) and SO249 BERING of R/V Sonne funded by the German Federal Ministry for Education and Research (BMBF), (ii) Lv63 of R/V Akademik Lavrentiev supported by grants #41420104005 and #40710069004 from the National Natural Science Foundation of China (NSFC). We acknowledge the GEOMAR Helmholtz Centre for Ocean Research Kiel for funding analytical studies and thank Mario Thöner (GEOMAR) for his assistance with EPMA, and Dieter Garbe-Schönberg and Ulrike Westernströer (both at Kiel University) for their assistance with LA-ICP-MS analyses. Visits by A.D. to Kiel for tephra analyses were funded by the Russian Foundation for Basic Research (RFBR) grant #11-05-00506 and the co-operative NSFC-RFBR grant #16-55-53048. We are grateful to Gene Yogodzinski for sharing his compilation of geochemical data on Aleutian rocks. Work on the manuscript was funded by the Russian Science Foundation grant #16-17-10035. We thank Kristi Wallace, Richard Brown, and Andrew Harris for their useful comments and English editing that substantially improved the quality of this manuscript.

## References

Alekseeva TN, Murdmaa IO, Ivanova EV, Ovsepyan EA, Kuz'mina TG, Seitkalieva EA (2015) Sedimentation in the submarine Shirshov ridge area (Bering Sea) during the last 180–185 ka (Penultimate glaciation-Holocene). Lithol Miner Resour 50(5):341–360

Alloway BV, Pillans BJ, Carter L, Naish TR, Westgate JA (2005) Onshore–offshore correlation of Pleistocene rhyolitic eruptions from New Zealand: implications for TVZ eruptive history and paleoenvironmental construction. Quat Sci Rev 24:1601–1622. https://doi.org/10.1016/j.quascirev.2004.07.026

Aoki K, Asahi H, Nagatsuma Y, Kurihara K, Fukuoka T, Sakamoto T, Iijima I (2012) Geochemical characters of Quaternary tephra beds and their stratigraphic position in the sedimentary core drilled at the site U1343 in the central Bering Sea. AGU Fall Meeting, San Francisco, CA, pp 3–7 December 2012. Abstract #V43B-2828

Arculus RJ (2003) Use and abuse of the terms calcalkaline and calcalkalic. J Petrol 44(5):929–935

Bindeman IN, Fournelle JH, Valley JW (2001) Low-δ 18 O tephra from a compositionally zoned magma body: Fisher caldera, Unimak Island, Aleutians. J Volcanol Geotherm Res 111:35–53. https://doi.org/10.1016/S0377-0273(01)00219-0

Blockley SP, Bourne AJ, Brauer A, Davies SM, Hardiman M, Harding PR et al (2014) Tephrochronology and the extended intimate (integration of ice-core, marine and terrestrial records) event stratigraphy 8-128 ka b2k. Quat Sci Rev 106:88–100

Braitseva OA, Ponomareva VV, Sulerzhitsky LD, Melekestsev IV, Bailey J (1997) Holocene key-marker tephra layers in Kamchatka Russia. Quat Res 47(2):125–139

Cameron CE and Nye CJ (2014) Preliminary database of Quaternary vents in Alaska: Alaska Division of Geological & Geophysical Surveys Miscellaneous Publication 153, 11 p. doi:https://doi.org/10.14509/27357

Cameron CE, Snedigar SF, Nye CJ (2014) Alaska Volcano Observatory Geochemical Database: Alaska Division of Geological & Geophys Surv Digital Data Series 8, https://www.avo.alaska.edu/geochem/index.php, doi:https://doi.org/10.14509/29120

Carson EC, Fournelle JH, Miller TP, Mickelson DM (2002) Holocene tephrochronology of the Cold Bay area, Southwest Alaska peninsula. Quat Sci Rev 21:2213–2228. https://doi.org/10.1016/S0277-3791(02)00023-9

Cook E, Portnyagin M, Ponomareva V, Bazanova L, Svensson A, Garbe-Schönberg D (2018) First identification of cryptotephra from the Kamchatka peninsula in a Greenland ice core: implications of a widespread marker deposit that links Greenland to the Pacific northwest. Quat Sci Rev 181:200–206. https://doi.org/10.1016/j.quascirev.2017.11.036

Coombs ML, Larsen JF, Neal CA (2018) Postglacial eruptive history and geochemistry of Semisopochnoi volcano, western Aleutian Islands. Alaska: US Geological Survey Scientific Investigations Report 2017–5150:33. https://doi.org/10.3133/sir20175150

Costa A, Smith V, Macedonio G, Matthews N (2014) The magnitude and impact of the youngest Toba Tuff super-eruption. Front Earth Sci 2. doi:https://doi.org/10.3389/feart.2014.00016

Coulter SE, Pilcher JR, Plunkett G, Baillie M, Hall VA, Steffensen JP, Vinther BM, Clausen HB, Johnsen SJ (2012) Holocene tephras highlight complexity of volcanic signals in Greenland ice cores. J Geophys Res-Atmos 117(D21), 16):D21303. https://doi.org/10.1029/2012JD017698

Creager JS, Scholl DW (1973) Initial reports of the deep sea drilling project, V.19. Washington (US Government Printing Office):913

Davies SM (2015) Cryptotephras: the revolution in correlation and precision dating. J Quat Sci 30:114–130. https://doi.org/10.1002/jqs.2766

Davies LJ, Jensen BJL, Froese DG, Wallace KL (2016) Late Pleistocene and Holocene tephrostratigraphy of interior Alaska and Yukon: key beds and chronologies over the past 30,000 years. Quat Sci Rev 146:28–53

Delong SE, Perfit MR, McCulloch MT, Ach J (1985) Magmatic evolution of Semisopochnoi Island, Alaska: trace-element and isotopic constraints. J Geol 93(5):609–618. https://doi.org/10.1086/628985

Derkachev AN, Portnyagin MV, Ponomareva VV, Gorbarenko SA, Malakhov MI, Nikolaeva NA, Nürnberg D, Shi Xuefa, Liu Yanguang (2015) Marker tephra layers of large explosive eruptions from volcanoes of Aleutian Islands and Alaska in Quaternary deposits of the Bering Sea. Geology of Seas and Oceans Proc XXI Int Conf on Marine Geol Moscow, Russia, November 16–20, 2015, vol I, 107–111 (in Russian) http://geoschool.ocean.ru/index.php/materialy/2017.html

Dullo WC, Baranov B, van den Bogaard C (2009) FS Sonne Fahrtbericht/cruise report SO201-2 KALMAR: Kurile-Kamchatka and ALeutian MARginal sea-island arc systems: geodynamic and climate interaction in space and time. Busan/Korea-Tomakomai/Japan 3008-0810: 2009 http://oceanrepgeomarde/7135/1/945_Dullo_2009_FsSonneFahrtberichtCruise_Monogr_pubid12967pdf

Elliott T, Plank T, Zindler A, White W, Bourdon B (1997) Element transport from slab to volcanic front at the Mariana arc. J Geophys Res 102(B7):14991–15019

Expedition 323 Scientists (2010) Bering Sea paleoceanography: Pliocene–Pleistocene paleoceanography and climate history of the Bering Sea. IODP Prel Rept 323 doi:https://doi.org/10.2204/iodp.pr.323.2010

Finney B, Turner S, Hawkesworth C, Larsen J, Nye C, George R, Bindeman I, Eichelberger J (2008) Magmatic differentiation at an island-arc caldera: Okmok volcano, Aleutian Islands, Alaska. J Petrol 49(5):857–884

GEOROC (Geochemistry of Rocks of the Oceans and Continents), http://www.georocmpch-mainzgwdgde/georoc/

Gersonde R (2012) The expedition of the research vessel “Sonne” to the Subpolar North Pacific and the Bering Sea in 2009 (SO202-INOPEX), in: Reports on Polar and Marine Research. Alfred Wegener Institute, Bremerhaven, p 323

Gill JB (1981) Orogenic andesites and plate tectonics. Springer-Verlag, Berlin-Heidelberg, p 390

Gorbarenko SA, Artyomova AV (2003) Chronostratigraphy of the Upper Quaternary sediments of the northwestern Pacific and the Bering Sea, change of the environment and productivity of the region. Tikhookeanskaya Geologiya (Pacific Geology) 22(5):23–38 (in Russian)

Gorbarenko SA, Basov IA, Chekhovskaya MP, Southon J (2005) Orbital and millennium scale environmental changes in the southern Bering Sea during last glacial–Holocene: geochemical and paleontological evidences. Deep-Sea Research II 52:2174–2185

Gorbarenko SA, Wang P, Wang R, Cheng X (2010) Orbital and suborbital environmental changes in the southern Bering Sea during last 50 kyr. Palaeogeogr Palaeoclimatol Palaeoecol 286:97–106. https://doi.org/10.1016/j.palaeo.2009.12.014

Graham RW, Belmecheri S, Choy K, Culleton BJ, Davies LJ, Froese D, Heintzman PD, Hritz C, Kapp JD, Newsom LA, Rawcliffe R (2016) Timing and causes of mid-Holocene mammoth extinction on St. Paul Island, Alaska. P Nat Acad Sci USA 113:9310–9314. https://doi.org/10.1073/pnas.1604903113

Harada N (ed) (2006) Cruise report, MR06–04, leg 1 and 2. JAMSTEC, Japan http://www.godac.jamstec.go.jp/catalog/data/doc_catalog/media/MR06-04_leg1-2_all.pdf

Hart SR, Staudigel H (1982) The control of alkalies and uranium in seawater by ocean crust alteration. Earth Planet Sci Lett 58:202–212

Jarosewich EJ, Nelen JA, Norberg JA (1980) Reference samples for electron microprobe analysis. Geostand Newslett 4(1):43–47

Jennings A, Thordarson T, Zalzal K, Stoner J, Hayward C, Geirsdóttir Á, Miller G (2014) Holocene tephra from Iceland and Alaska in SE Greenland shelf sediments. Geol Soc London Spec Pub - Marine Tephrochronol 398(1):157–193

Jensen BJL, Froese DG, Preece SJ, Westgate JA, Stachel T (2008) An extensive middle to Late Pleistocene tephrochronologic record from east-Central Alaska. Quat Sci Rev 27(3–4):411–427

Jensen BJL, Preece SJ, Lamothe M, Pearce NJG, Froese DG, Westgate JA, Schaefer J, Begét J (2011) The variegated (VT) tephra: a new regional marker for middle to late marine isotope stage 5 across Yukon and Alaska. Quat Int 246(1–2):312–323

Jensen BJL, Reyes AV, Froese DG, Stone DB (2013) The palisades is a key reference site for the middle Pleistocene of eastern Beringia: new evidence from paleomagnetics and regional tephrostratigraphy. Quat Sci Rev 63:91–108

Jochum KP, Stoll B, Herwig K, Willbold M, Hofmann AW, Amini M, Aarburg S, Abouchami W, Hellebrand E, Mocek B, Raczek I (2006) MPI-DING reference glass for in situ microanalysis: new reference values for element concentrations and isotope ratios. Geochem Geophys Geosyst 7:Q02008. https://doi.org/10.1029/2005GC001060

Jochum KP, Nohl U (2008) Reference materials in geochemistry and environmental research and the GeoReM database. Chem Geol 253(1):50–53. https://doi.org/10.1016/j.chemgeo.2008.04.002

Katoh S, Nagaoka S, WoldeGabriel G, Renne P, Snow MG, Beyene Y, Suwa G (2000) Chronostratigraphy and correlation of the Plio-Pleistocene tephra layers of the Konso formation, southern main Ethiopian rift, Ethiopia. Quat Sci Rev 19(13):1305–1317. https://doi.org/10.1016/S0277-3791(99)00099-2

Kaufman DS, Jensen BJL, Reyes AV, Schiff CJ, Froese DG, Pearce NJG (2012) Late Quaternary tephrostratigraphy, Ahklun Mountains, SW Alaska. J Quat Sci 27:344–359. https://doi.org/10.1002/jqs.1552

Kay SM, Kay RW (1994) Aleutian magmas in space and time. In: Plafker G, Berg HC (eds) The geology of Alaska, Geological Society of America, doi:https://doi.org/10.1130/DNAG-GNA-G1.687

Kelemen PB, Hangøj K, Greene AR (2003a) One view of the geochemistry of subduction-related magmatic arcs, with an emphasis on primitive andesite and lower crust. In: Treatise on geochemistry, vol 3 Elsevier, pp 593–659

Kelemen PB, Yogodzinski GM, Scholl DW (2003b) Along-strike variations in the Aleutian Island arc: genesis of high Mg# andesite and implications for continental crust. In: Inside the subduction Factory, Geophysical Monograph 138, American Geophysical Union, pp 223–276

Kuehn H, Lembke-Jene L, Gersonde R, Esper O, Lamy F, Arz H, Kuhn G, Tiedemann R (2014) Laminated sediments in the Bering Sea reveal atmospheric teleconnections to Greenland climate on millennial to decadal timescales during the last deglaciation. Clim Past 10(6):2215–2236

Kutterolf S, Freundt A, Perez W, Morz T, Schacht U, Wehrmann H, Schmincke HU (2008a) Pacific offshore record of plinian arc volcanism in Central America: 1 along-arc correlations. Geochem Geophy Geosy 9. doi:https://doi.org/10.1029/2007gc001631

Kutterolf S, Freundt A, Perez W (2008b) Pacific offshore record of plinian arc volcanism in Central America: 2 tephra volumes and erupted masses. Geochem Geophy Geosy 9. doi:https://doi.org/10.1029/2007gc001791

Kyle PR, Ponomareva VV, Schluep RR (2011) Geochemical characterization of marker tephra layers from major Holocene eruptions, Kamchatka peninsula, Russia. Int Geol Rev 53(9):1059–1097. https://doi.org/10.1080/00206810903442162

Larsen JF, Neal CA, Schaefer JG, Beget J, Nye CJ (2007) Late Pleistocene and Holocene caldera-forming eruptions of Okmok caldera, Aleutian Islands, Alaska. In: Eichelberger J, Gordeev E, Izbekov P, Kasahara M, Lees J (Eds), Volcanism and subduction: the Kamchatka region, American Geophysical Union, Geophys Monograph Ser 172: 343–364

Larsen JF, Śliwiński MG, Nye C, Cameron C, Schaefer JR (2013) The 2008 eruption of Okmok volcano, Alaska: petrological and geochemical constraints on the subsurface magma plumbing system. J Volcanol Geotherm Res 264:85–106

Le Bas MJ, Le Maitre RW, Streckeisen A, Zanettin B (1986) A chemical classification of volcanic-rocks based on the total alkali-silica diagram. J Petrol 27(3):745–750

Legros F (2000) Minimum volume of a tephra fallout deposit estimated from a single isopach. J Volcanol Geotherm Res 96(1–2):25–32

Lowe DJ (2011) Tephrochronology and its application: a review. Quat Geochronol 6(2):107–153

Lowe DJ, Pearce NJ, Jorgensen MA, Kuehn SC, Tryon CA, Hayward CL (2017) Correlating tephras and cryptotephras using glass compositional analyses and numerical and statistical methods: review and evaluation. Quat Sci Rev 175:1–44

Mason BG, Pyle DM, Oppenheimer C (2004) The size and frequency of the largest explosive eruptions on earth. Bull Volcanol 66(8):735–748. https://doi.org/10.1007/s00445-004-0355-9

Max L, Riethdorf JR, Tiedemann R, Smirnova M, Lembke-Jene L, Fahl K, Nürnberg D, Matul A, Mollenhauer G (2012) Sea surface temperature variability and sea-ice extent in the subarctic Northwest Pacific during the past 15,000 years. Paleoceanogr Paleoceanol 27(3). https://doi.org/10.1029/2012PA002292

McDonough WF, Sun S-S (1995) The composition of the earth. Chem Geol 120:223–253

Miller TP, Smith RL (1987) Late Quaternary caldera-forming eruptions in the eastern Aleutian arc, Alaska. Geology 15(5):434–438

Miyashiro A (1975) Volcanic rock series and tectonic setting. Annu Rev Earth Planet Sci 3(1):251–269

Moll-Stalcup EJ (1994) Latest cretaceous and Cenozoic magmatism in mainland Alaska in: Plafker G, Berg HC (eds) the geology of Alaska: Boulder, Colorado, Geological Society of America, The Geology of North America, Volume G-1, pp 589–619

Neal CA, Larsen JF, Schaefer J (2009) The July-August 2008 hydrovolcanic eruption of Okmok volcano, Umnak Island, Alaska. Alaska Geol Soc Newslett 39(5):1–3

Newhall CG, Self S (1982) The volcanic explosivity index (VEI) an estimate of explosive magnitude for historical volcanism. J Geophys Res Oceans 87(C2):1231–1238

Nye CJ, Begét JE, Layer PW, Mangan MT, McConnell VS, McGimsey RG, Miller TP, Moore RB, Stelling PL (2018) Geochemistry of some quaternary lavas from the Aleutian Arc and Mt Wrangell: Alaska Division of Geological & Geophysical Surveys Raw Data File 2018–1, 29 doi:https://doi.org/10.14509/29843

Pearce JA, Parkinson IJ (1993) Trace element models for mantle melting: application to volcanic arc petrogenesis in: Prichard HM, Alabaster T, Harris NB, Neary CR (eds) magmatic processes and plate tectonics, vol 76 geological society special publication, pp 373–403

Pearce C, Varhelyi A, Wastegård S, Muschitiello F, Barrientos N, O'Regan M, Cronin TM, Gemery L, Semiletov I, Backman J, Jakobsson M (2017) The 36 ka Aniakchak tephra in the Arctic Ocean: a constraint on the Holocene radiocarbon reservoir age in the Chukchi Sea. Clim Past 13(4):303–316

Pearce NJG, Westgate JA, Preece SJ, Eastwood WJ, Perkins WT (2004) Identification of Aniakchak (Alaska) tephra in Greenland ice core challenges the 1645 BC date for Minoan eruption of Santorini. Geochem Geophys Geosyst 5(3):Q03005. https://doi.org/10.1029/2003GC000672

Plunkett G, Coulter SE, Ponomareva VV, Blaauw M, Klimaschewski A, Hammarlund D (2015) Distal tephrochronology in volcanic regions: challenges and insights from Kamchatkan lake sediments. Glob Planet Chang 134:26–40. https://doi.org/10.1016/j.gloplacha.2015.04.006

Ponomareva V, Portnyagin M, Derkachev A, Juschus O, Garbe-Schönberg D, Nürnberg D (2013a) Identification of a widespread Kamchatkan tephra: a middle Pleistocene tie-point between Arctic and Pacific paleoclimatic records. Geophys Res Lett 40(14):3538–3543. https://doi.org/10.1002/grl.50645

Ponomareva V, Portnyagin M, Derkachev A, Pendea IF, Bourgeois J, Reimer PJ, Garbe-Schönberg D, Krasheninnikov S, Nürnberg D (2013b) Early Holocene M~6 explosive eruption from Plosky volcanic massif (Kamchatka) and its tephra as a link between terrestrial and marine paleoenvironmental records. Int J Earth Sci 102:1673–1699. https://doi.org/10.1007/s00531-013-0898-0

Ponomareva V, Portnyagin M, Pevzner M, Blaauw M, Kyle P, Derkachev A (2015a) Tephra from andesitic Shiveluch volcano, Kamchatka, NW Pacific: chronology of explosive eruptions and geochemical fingerprinting of volcanic glass. Int J Earth Sci 104(5):1459–1482

Ponomareva V, Portnyagin M, Davies S (2015b) Tephra without borders: far-reaching clues into past explosive eruptions. Front Earth Sci/Volcanol 3:83. https://doi.org/10.3389/feart.2015.00083

Ponomareva V, Portnyagin M, Pendea F, Zelenin E, Bourgeois J, Pinegina T, Kozhurin A (2017) A full Holocene tephrochronology for the Kamchatsky peninsula region: applications from Kamchatka to North America. Quat Sci Rev 168:101–122. https://doi.org/10.1016/j.quascirev.2017.04.031

Ponomareva V, Polyak L, Portnyagin M, Abbott P, Zelenin E, Vakhrameeva P, Garbe-Schönberg D (2018) Holocene tephra from the Chukchi-Alaskan margin. Arctic Ocean: Implications for sediment chronostratigraphy and volcanic history Quat Geochronol 45: 85–97. https://doi.org/10.1016/j.quageo.2017.11.001

Preece SJ, Westgate JA, Stemper BA, Pewe TL (1999) Tephrochronology of Late Cenozoic loess at Fairbanks. Central Alaska Geol Soc Am Bull 111(1):71–90

Preece SJ, Pearce NJG, Westgate JA, Froese DG, Jensen BJL, Perkins WT (2011a) Old crow tephra across eastern Beringia: a single cataclysmic eruption at the close of marine isotope stage 6. Quat Sci Rev 30:2069–2090. https://doi.org/10.1016/j.quascirev.2010.04.020

Preece SJ, Westgate JA, Froese DG, Pearce NJG, Perkins WT (2011b) A catalogue of late Cenozoic tephra beds in the Klondike goldfields and adjacent areas, Yukon territory. Yukon geological survey contribution 010. Can J Earth Sci 48:1386–1418. https://doi.org/10.1139/e10-110

Pyle DM (1995) Mass and energy budgets of explosive volcanic eruptions. Geophys Res Lett 22:563–566. https://doi.org/10.1029/95GL00052

Pyne-O'Donnell SDF, Hughes PDM, Froese DG, Jensen BJL, Kuehn SC, Mallon G, Amesbury MJ, Charman DJ, Daley TJ, Loader NJ, Mauquoy D, Street-Perrott FA, Woodman-Ralph J (2012) High-precision ultra-distal Holocene tephrochronology in North America. Quat Sci Rev 52:6–11. https://doi.org/10.1016/j.quascirev.2012.07.024

Rawson H, Naranjo JA, Smith V, Fontijn K, Pyle DM, Mather TA et al (2015) The frequency and magnitude of post-glacial explosive eruptions at Volcán Mocho-Choshuenco, southern Chile. J Volcanol Geotherm Res 299:103–129. https://doi.org/10.1016/j.jvolgeores.2015.04.003

Reeder JW (1990) Sugarloaf. Annual report of the world volcanic eruptions in 1987. Bulletin of Vol Erup 27:36

Riethdorf J-R, Nürnberg D, Max L, Tiedemann R, Gorbarenko SA, Malakhov MI (2013) Millennial scale variability of marine productivity and terrigenous matter supply in the western Bering Sea over the past 180 kyr. Clim Past 9(3):1345–1373. https://doi.org/10.5194/cp-9-1345-2013

Rocholl A (1998) Major and trace element composition and homogeneity of microbeam reference material: basalt glass USGS BCR-2G. Geostandards Newslett: J Geostandards and Geoanalysis 22:33–45

Seliverstov NI, Gavrilenko GM, Kir'yanov VY (1989) Signs of the recent activity of the submarine Piip volcano, Komandorsky Basin. Vulkanologia i Seysmologia (Volcanology and Seismology) 6:3–18 (in Russian)

Shane PA (2000) Tephrochronology: a New Zealand case study. Earth Sci Rev 49(1–4):223–259

Shane P, Wright IC (2011) Late Quaternary tephra layers around Raoul and Macauley Islands, Kermadec arc: implications for volcanic sources, explosive volcanism and tephrochronology. J Quat Sci 26:422–432. https://doi.org/10.1002/jqs.1468

Takahashi K, Ravelo AC, Alvarez Zarikian CA and the Expedition 323 Scientists (2011) Proc IODP, 323: Tokyo (Integrated Ocean Drilling Program Manag Int, Inc) doi:https://doi.org/10.2204/iodp.proc.323.2011

Wallace KL, Hayden LA, Neal CA (2017) Major-element glass compositions of tephra from the circa 36 ka eruption of Aniakchak volcano, Alaska peninsula. Alaska: Alaska Division of Geological & Geophysical Surveys Raw Data File 2017-9:9. https://doi.org/10.14509/29777

Werner R, Hoernle K, Hauff F, Portnyagin M, Yogodzinski G, Ziegler A (2016) RV SONNE Fahrtbericht / Cruise Report SO249 BERING – Origin and Evolution of the Bering Sea: An Integrated Geochronological, Volcanological, Petrological and Geochemical Approach In, vol GEOMAR Research Centre for Ocean Research Kiel, Kiel, pp 451

Westgate JA, Preece SJ, Kotler E, Hall S (2000) Dawson tephra; a prominent stratigraphic marker of Late Wisconsinan age in west-central Yukon, Canada. Can J Earth Sci 37(4):621–627

Wirth KR, Grandy J, Kelley K, Sadofsky S (2002) Evolution of crust and mantle beneath the Bering Sea region: evidence from xenoliths and the late Cenozoic basalts. In: Miller EL, Grantz A, Klemperer SL (eds) Tectonic evolution of the Bering shelf - Chukchi Sea- Arctic margin and adjacent landmasses, vol 360. Geological Society of America Special Paper, Boulder, Colorado, pp 167–193

Wood, ChA, Kienle J (Eds) (1990) Volcanoes of North America: United States and Canada Cambridge University Press

Yogodzinski GM, Volynets ON, Koloskov AV, Seliverstov NI, Matvenkov VV (1994) Magnesian andesites and the subduction component in a strongly calc-alkaline series at Piip volcano, Far Western Aleutians. J Petrol 35(1):163–204

Yogodzinski GM, Brown ST, Kelemen PB, Vervoort JD, Portnyagin M, Sims KWW, Hoernle K, Jicha BR, Werner R (2015) The role of subducted basalt in the source of island arc magmas: evidence from seafloor lavas of the Western Aleutians. J Petrol 56(3):441–492. https://doi.org/10.1093/petrology/egv006